Optical Differential Phase Modulation:

System Modeling and Performance

Lei Wang

A Thesis

In

The Department of Electrical and Computer Engineering

Presented in Partial Fulfillment of the Requirements for the Degree of Master of

Applied Science at

Concordia University

Montreal, Quebec, Canada

December 2004

Your file Votre référence
ISBN: 0-494-04403-9
Our file Notre référence
ISBN: 0-494-04403-9

Abstract

Optical Differential Phase Modulation: System Modeling and Performance

Lei Wang

We investigated high speed optical fiber communication systems using optical π -DPSK, $\pi/2$ -DPSK, DQPSK and Offset-DQPSK modulation techniques, focusing on the system modeling and comparison of performance. The electronic precoder of optical $\pi/2$ -DPSK was yet unknown, and its logic and basic circuit are presented in this thesis. We also compared the system performance with the impact of inter symbol interference (ISI) caused by fiber nonlinear effect, narrowband inline optical filtering and residual chromatic dispersion. It is shown that DQPSK has the narrowest signal bandwidth among four phase modulation schemes; Offset-DQPSK has two main lobes in its optical spectrum; Offset-DQPSK has the best tolerance to ISI induced by fiber nonlinear effect; π-DPSK has the best tolerance to optical filtering; and DQPSK has the best tolerance to residual chromatic dispersion. π-DPSK has better tolerance to residual chromatic dispersion than $\pi/2$ -DPSK. All of these works were verified on Optism, a commercial optical simulation software platform.

Acknowledgements

I am deeply grateful to my supervisor Dr. **John Xiupu Zhang** for his initiating this project, and for his research advices, his teaching and inspiration in all phases of this research work. Many thanks and appreciation is due to my family and friends for their encouragement and moral support.

Related Publication

Xiupu Zhang, Guodong Zhang, Chongjin Xie, Lei Wang, "Noise statistics in optically preamplified differential phase shift keying receiver with Mach-Zehnder interferometer demodulation." *Optics letters Vol. 29, No. 4, pp.337-339, 2004.*

Contents

List of Symbols and Acronyms

DPSK	Differential phase shift keying
DQPSK	Differential quadrature phase shift keying
Offset-DQPSK	Offset differential quadrature phase shift keying
CSRZ	Carrier-suppressed return-to-zero
OOK	On-off keying
MZM	Mach-Zehnder Modulator
MZI	Mach-Zehnder delay interferometer demodulation
CD	Chromatic dispersion
SPM	Self phase modulation
XPM	Cross phase modulation
DWDM	Dense wavelength division multiplex
ASE	Amplified spontaneous emission
$\Delta\phi$	Phase difference between successive symbols
ISI	Inter-symbol-interference
CW	Continuous wave
E_{in}	Electric field of input optical signal
E_{out}	Electric field of output optical signal

ρ	Splitting ratio of an optical couple
V_π	Voltage swing that generates a π (180°) phase shift
ω_c	Radian frequency of optical carrier
RZ	Return to zero
DC	Direct current
P_{input}	Input optical power of a pulse
FWHM	Full width at half maximum
τ	Time delay
$\Delta\theta_1, \Delta\theta_2$	Phase difference of two successive pulses relative to the laser carrier
R	Responsivity of the photodiode
SNR	Signal to noise ratio
PRBS	Pseudorandom bit sequence
SBSR	Side band suppression ratio
SMF	Single mode fiber
DCF	Dispersion compensation fiber
VOA	Variable optical attenuator
TDSS	Time Domain Split-Step

Chapter 1

Introduction

Due to the explosive growth of communication traffic, there is a substantial effort to increase the transmission capacity of light wave systems. High spectral efficiency techniques are attractive since they offer a way to achieve high capacities with existing link. Once the transmission rate is increased to 40 Gb/s from 10 Gb/s, a number of challenges and additional transmission penalties arise. In order to minimize the penalties imposed by the increased bit rate, some new modulation formats have been proposed and investigated, such as optical duobinary, modified optical duobinary [1-7], carrier-suppressed return-to-zero (CSRZ) on-off keying (OOK) [6-12], and differential phase shift keying (DPSK) [13-25].

In this thesis, we consider differential phase shift keying modulation. DPSK is spectral condensed modulation scheme which has some unique properties that make it suitable to resist bandwidth related impairments like fiber chromatic dispersion (CD). The constant intensity envelope of DPSK signal makes it a good modulation scheme to resist fiber nonlinear effect, such as self phase modulation (SPM) in single optical channel and cross phase modulation (XPM) in dense wavelength division

multiplexing (DWDM) optical system. On the other hand, in high speed transmission system which bit rates are more than 10 Gb/s, the optically amplified spontaneous emission (ASE) noise introduces not only linear phase noise, but also a strong nonlinear phase noise which is the combined effect of the ASE noise with fiber nonlinearity. Investigations of receiver sensitivity and nonlinear performance in optical phase modulation have become a hot topic since year 2000.

DPSK is a class of modulation techniques encoding information in the phase difference $\Delta\phi$ between successive symbols. According the value set of $\Delta\phi$, we have π-DPSK [13-25], $\pi/2$-DPSK [26-29], DQPSK [30-36], and Offset-DQPSK [37-41]. These four modulation schemes are feasible in optical transmission system. The modeling and performance comparison of these modulation schemes were performed mostly in satellite communication during the 1980s [41-42]. We investigated these modulation schemes in optical domain. We give detailed system configuration modeling including both physical optical configuration and logical electronic precoder. The electronic precoder of optical $\pi/2$-DPSK is yet unknown until now; we presented its logic and basic circuit in this thesis. We compared the system performance under inter-symbol-interference (ISI) impairments of fiber nonlinear effect, narrowband inline optical filter and chromatic dispersion.

In [26] the impact of CD (chromatic dispersion) and PMD (polarization modulation dispersion) in power penalties of π-DPSK and $\pi/2$-DPSK, is compared, and it was founds that with either weak or strong optical filtering π-DPSK has lower CD penalties than $\pi/2$-DPSK. This conclusion is consistent with our result which will be given in Chapter 4. For Offset-DQPSK, we cannot obtain the correct eye diagram

based on the model of Offset-DQPSK proposed in [37]; and it is verified that the transmission data cannot be correctly demodulated. Moreover, optical spectrum of Offset-DQPSK we obtained also differs from [37]. The impacts of nonlinear effect and residual chromatic dispersion for Offset-DQPSK and DQPSK were compared in [37]. It was found that Offset-DQPSK has the same robustness to fiber nonlinear effect as DQPSK. But we found that the optimum launched power was not investigated with the consideration of fiber nonlinear effect. It was found that Offset-DQPSK is slightly worse than DQPSK in tolerance to residual chromatic dispersion. Furthermore, electronic precoder of optical DQPSK in [45] is consistent to this thesis.

All works in our thesis were carried out on Optism, a commercial optical simulation software platform (See Appendix A). Some theoretical analyses are not included in this thesis, we leave them open for our future works.

The rest of this thesis is organized as follows: In Chapter 2, we present some particular optical components used in optical differential phase shift keying system. In Chapter 3, we comprehensively give system modeling of four optical phase shift modulation. Precoders are illustrated in Chapter 3. In Chapter 4, we compare variance of aspect of system performances of those four systems.

Chapter 2

Optical phase modulator and demodulator

In optical phase shift keying (PSK) communication system, the laser diode is biased at a constant current to provide the CW laser output, and an optical modulator placed next to the laser diode converts the CW light into a data coded pulse train with the right modulation format. The optical power keeps constant in every bit period, every optical pulse has different phase according to the data to be transmitted. After fiber link transmission, phase modulated signal interferes with another light, and is converted to optical intensity modulation signal, and then a direct detection technique can be used to recover the data information.

In high speed optical transmission system, Mach-Zehnder modulator (MZM) and Mach-Zehnder delay interferometer (MZI) are unique components used in optical phase modulation technique. In this chapter, we review some basic optical components used in high speed modulation scheme. We give conceptual model of each component. These models are fundamental knowledge in our simulation process.

2.1 Mach-Zehnder Modulator (MZM)

2.1.1 Coupler

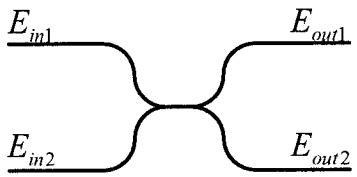

Figure 1: Optical coupler.

Figure 1 shows the structure of an optical coupler. The action of a fiber coupler is governed by the matrix equation of $E_{out} = TE_{in}$, where T is the 2×2 transfer matrix and E is a column vector whose two components represent the input (or output) optical fields at the two ports. For an ideal coupler, the transfer matrix T should be both unitary and symmetric, the unitary holds for a lossless coupler and the symmetric requirement results from time reversal property of light. Thus the most general form of this matrix is $T=\begin{pmatrix} a & b \\ b & a \end{pmatrix}$, with the property of $a^2-b^2=1$. At the same time, $|a^2|+|b^2|=1$ is imposed because the total power does not change during splitting. We can take a to be real. Then, these two requirements are met only if $a=\sqrt{\rho}$ and $b=-j\sqrt{1-\rho}$. So we get

$$\begin{pmatrix} E_{out1} \\ E_{out2} \end{pmatrix} = \begin{pmatrix} \sqrt{\rho} & -j\sqrt{1-\rho} \\ -j\sqrt{1-\rho} & \sqrt{\rho} \end{pmatrix} \begin{pmatrix} E_{in1} \\ E_{in2} \end{pmatrix} \tag{2.1}$$

For an ideal case $|a|=|b|=\sqrt{1/2}$, that means the power of two output arms are equal. This kind of coupler is usually used as a power splitter, and it is also called 3 dB coupler. The matrix of a 3 dB coupler is

$$\begin{pmatrix} E_{out1} \\ E_{out2} \end{pmatrix} = \begin{pmatrix} \sqrt{0.5} & -j\sqrt{0.5} \\ -j\sqrt{0.5} & \sqrt{0.5} \end{pmatrix} \begin{pmatrix} E_{in1} \\ E_{in2} \end{pmatrix} \tag{2.2}$$

2.1.2 Optical $LiNbO_3$ phase modulator

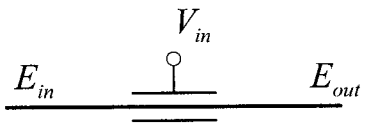

Figure 2: Optical phase modulator.

Figure 2 shows the structure of an optical $LiNbO_3$ phase modulator. It is an optical integrate device which incorporate light guiding channels in the $LiNbO_3$ crystal with higher refractive index than the surrounding medium. The refractive index of $LiNbO_3$ crystal can be changed based on electro-optic effect. The transfer function in terms of phase shift versus applied voltage is supposed to be linear:

$$E_{out} = e^{j\theta} E_{in} \tag{2.3}$$

where $\theta = \pi\left(\frac{V_{in}}{V_\pi}\right)$, V_π is the input voltage swing that generates a $\pi\,(180°)$ phase shift on the optical signal. This is a good approximation for realistic phase modulators based on the electro-optic effect in $LiNbO_3$ devices

Actually the nonlinear property of $LiNbO_3$ device and imperfect driven voltage impose strong modulation chirp, which narrows the modulation bandwidth. This defect of $LiNbO_3$ phase modulator makes it impossible to be used in high speed transmission system directly

2.1.3 Optical Mach-Zehnder Modulator (MZM)

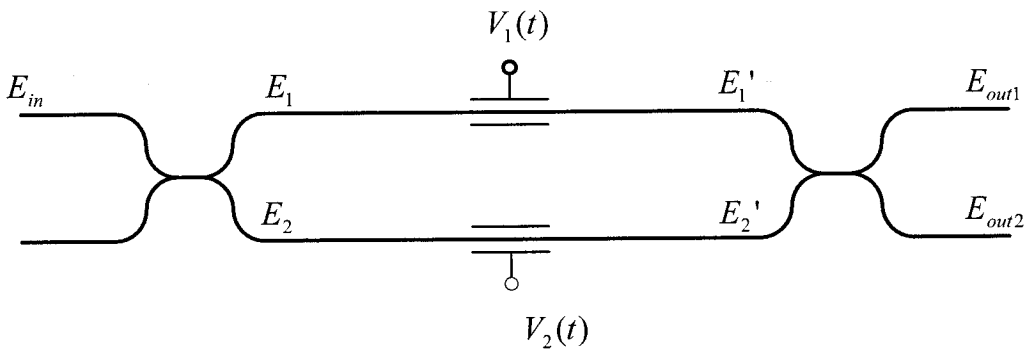

Figure 3: Optical Mach-Zehnder modulator.

Figure 3 shows dual arm optical Mach-Zehnder Modulator. E_{in} is electric field of input optical signal. E_1 and E_2 are outputs of first optical coupler. $V_1(t)$ and $V_2(t)$ are driving voltages of two $LiNbO_3$ phase modulators. E_1' and E_2' are output optical signals of two phase modulator. E_{out1} and E_{out1} are outputs of the MZM.

A dual-arm MZM is constructed by connecting two 3 dB optical couplers in series with each arm making use of the $LiNbO_3$ material as a phase modulator. The first coupler splits the input signal into two equal parts. In the absence of external voltage of the two arms, the optical fields in the two arms of the MZM experience identical phase shifts and interfere constructively and destructively at each output of the second coupler, respectively. The additional phase shift introduced in either one of the arms through voltage induced index changes destroys the state of interference.

The input optical electric field is represented as $E_{in} = |E_o| e^{j\omega_c t}$; where $|E_o|$ is optical

electric field amplitude; ω_c is radian frequency of optical carrier. We ignore the laser spectrum here. In this instance we adopt the exponential representation of the time varying part of the optical electric field. The first 3 dB coupler splits E_{in} into E_1 and E_2:

$$\begin{pmatrix} E_1 \\ E_2 \end{pmatrix} = \begin{pmatrix} \sqrt{\frac{1}{2}} & -j\sqrt{\frac{1}{2}} \\ -j\sqrt{\frac{1}{2}} & \sqrt{\frac{1}{2}} \end{pmatrix} \bullet \begin{pmatrix} E_{in} \\ 0 \end{pmatrix} \tag{2.4}$$

Consider the transfer function of an ideal $LiNbO_3$ phase modulator, $E_1' = E_1 e^{j\theta_1}$ and $E_2' = E_2 e^{j\theta_2}$. The second 3 dB coupler combines E_1' and E_2', and E_{out1} and E_{out2} are given by

$$\begin{pmatrix} E_{out1} \\ E_{out2} \end{pmatrix} = \begin{pmatrix} \sqrt{\frac{1}{2}} & -j\sqrt{\frac{1}{2}} \\ -j\sqrt{\frac{1}{2}} & \sqrt{\frac{1}{2}} \end{pmatrix} \bullet \begin{pmatrix} E_1' \\ E_2' \end{pmatrix} \tag{2.5}$$

After calculation we have

$$E_{out1} = 0.5E_{in}e^{j\theta_1} - 0.5E_{in}e^{j\theta_2} = jE_{in}\sin\frac{\theta_1 - \theta_2}{2}\exp\left(j\frac{\theta_1 + \theta_2}{2}\right) \tag{2.6a}$$

$$E_{out2} = -j0.5E_{in}e^{j\theta_1} - j0.5E_{in}e^{j\theta_2} = -E_{in}\cos\frac{\theta_1 - \theta_2}{2}\exp\left(j\frac{\theta_1 + \theta_2}{2}\right) \tag{2.6b}$$

E_{out1} and E_{out2} in Equation (2.6) shows that MZM can be used either as an amplitude modulator or a phase modulator.

When two arms of the MZM are push-pull driven, that is $\theta_1 = -\theta_2$, we obtain $E_{out1} = jE_{in}\sin\frac{\theta_1 - \theta_2}{2}$ and $E_{out2} = -E_{in}\cos\frac{\theta_1 - \theta_2}{2}$, that is amplitude modulation.

Sometimes $E_{out1} = jE_{in}\sin\frac{\theta_1 - \theta_2}{2}$ was called sine arm and $E_{out2} = -E_{in}\cos\frac{\theta_1 - \theta_2}{2}$ was called cosine arm.

When two arms of the MZM have equal electronic driving voltage, that is $\theta_1 = \theta_2$, we have $E_{out1} = 0$ and $E_{out2} = -E_{in}\exp\left(j\frac{\theta_1 + \theta_2}{2}\right)$. We can see that the cosine arm have the same optical power as the input except $\theta_1 = \theta_2$ phase shift, and the other arm have no power.

2.2 Optical pulse carvers

A pulse carver is used to carve return zero (RZ) pulses. RZ formats are more robust to inter symbol interference (ISI) introduced from transmission impairments, typically having lower sensitivity than their NRZ equivalents. MZM operating in the amplitude modulation condition is a popular method to construct an optical pulse carver.

Figure 4 shows the schematic of optical pulse carver. A MZM is driven with push-pull operation by a sine wave voltage, $V_1 = -V_2 = \frac{V_\pi}{2}\sin(\omega_p t)$, V_π - the π phase shift voltage of $LiNbO_3$ waveguide, and ω_p - frequency of the sine wave. The sine wave voltage introduces phase change on each arm, $\theta_1 = \pi\left(\frac{V_1}{V_\pi}\right) = \frac{\pi}{2}\sin(\phi)$ and

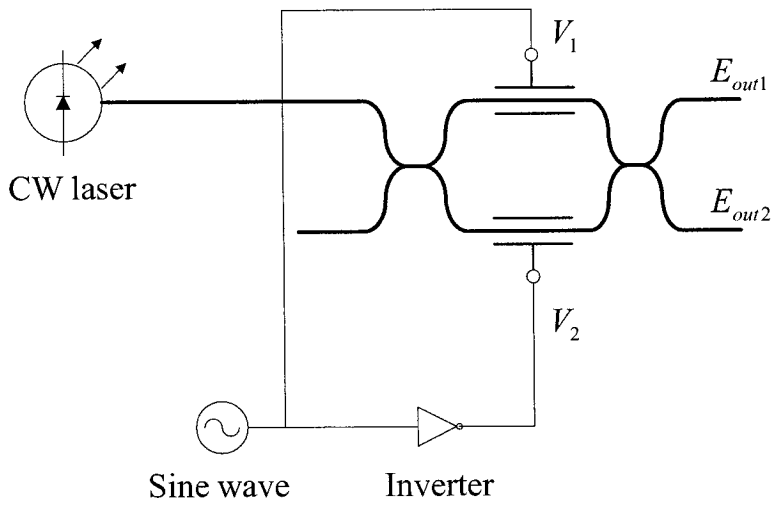

Figure 4: Schematic of optical pulse carver.

$\theta_2 = \pi\left(\frac{V_2}{V_\pi}\right) = -\frac{\pi}{2}\sin(\phi)$. By using Equation (2.6), we get:

$$E_{out1} = jE_{in}\sin\left(\frac{\pi}{2}\sin(\phi)\right) \tag{2.7a}$$

$$E_{out2} = -E_{in}\cos\left(\frac{\pi}{2}\sin(\phi)\right) \tag{2.7b}$$

We see that two out ports have different pulse shape and power. In order to tune the pulse shape, a bias DC voltage can be superposed into the sine wave. Figure 5 gives two approaches to superpose a DC voltage. All these two methods are meant to have a constant $\pi/2$ phase shift in the amplitude modulation, and there we have

$$E_{out1} = jE_{in}\sin\frac{\theta_1 - \theta_2 + \pi}{2} = jE_{in}\cos\left(\frac{\pi}{2}\sin(\phi)\right) \tag{2.8a}$$

$$E_{out2} = -E_{in}\cos\frac{\theta_1 - \theta_2 + \pi}{2} = -E_{in}\sin\left(\frac{\pi}{2}\sin(\phi)\right) \tag{2.8b}$$

Comparing Equations (2.8) and (2.7), we see that two arms exchange its modulation status after biased.

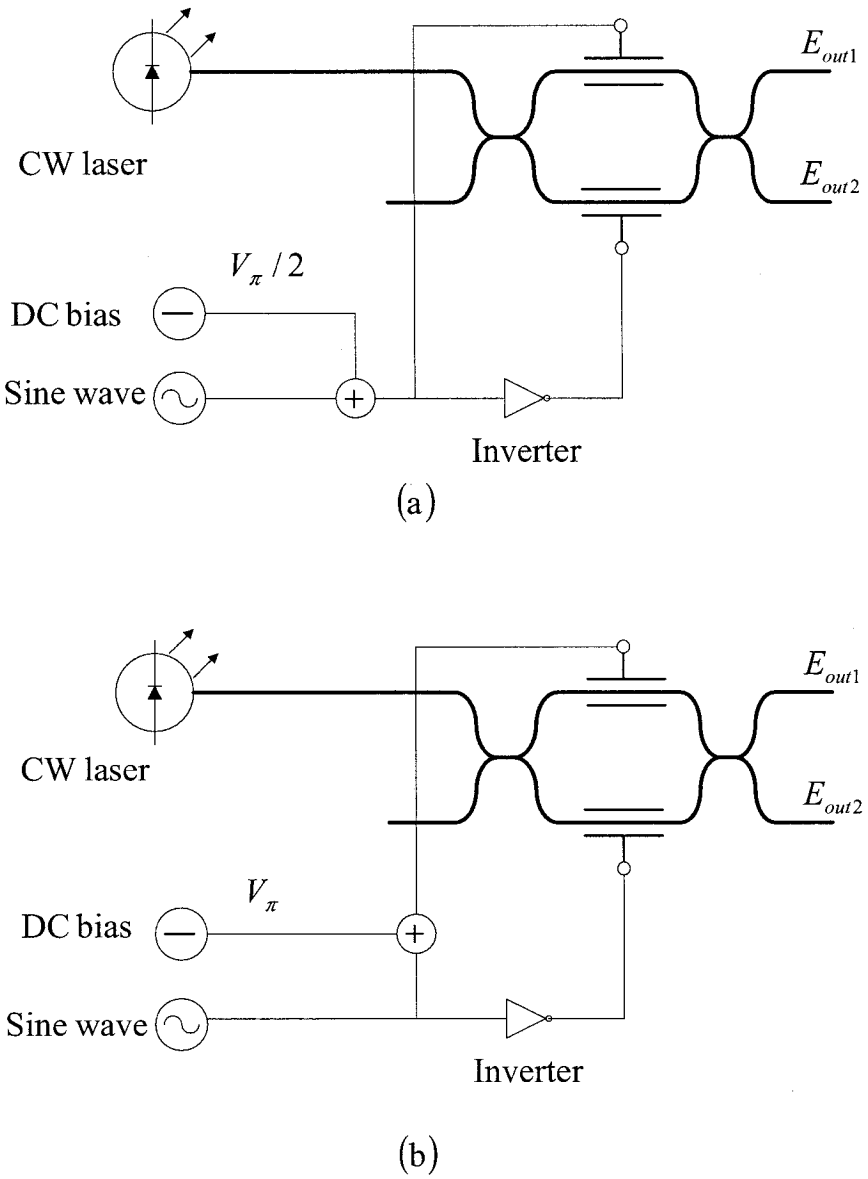

Figure 5: Schematic of unbalanced pulse carver with (a) both arm bias with a $V_\pi / 2$ voltage; and (b) single arm bias with a V_π voltage.

2.21 33% duty cycle pulse carver

The power representation of the sine arm by using $E_{out} = E_{in} \cos\left(\frac{\pi}{2}\sin(\phi)\right)$ is $P_{output} = P_{input}\left(\cos\left(\frac{\pi}{2}\sin(\phi)\right)\right)^2$, where P_{input} is the optical power of E_{in}. Its

normalized waveform is shown in Figure 6.

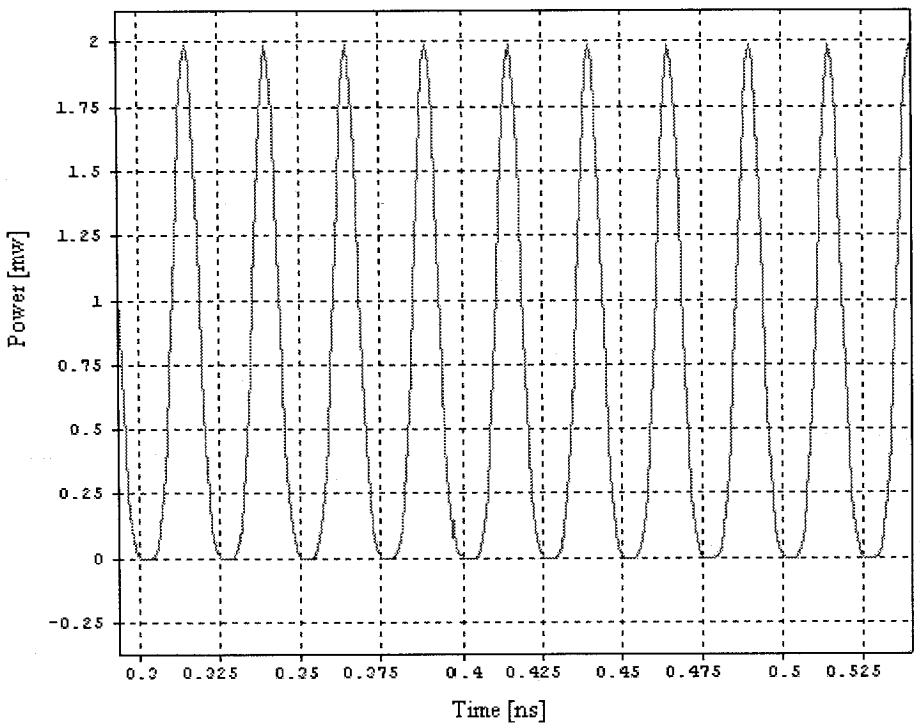

Figure 6: 33% duty cycle pulse carver at bit rate of 40 Gb/s.

The full width at half maximum (FWHM) of the pulse is 33%, and its peak to peak width is half of the cycle period of the sinusoidal wave of driving voltage.

2.22 66% duty cycle pulse carver

The power representation of the cosine arm by using $E_{out} = E_{in} \sin\left(\frac{\pi}{2}\sin(\phi)\right)$ is

$P_{output} = P_{input}\left(\sin\left(\frac{\pi}{2}\sin(\phi)\right)\right)^2$. Its normalized waveform is shown in Figure 7.

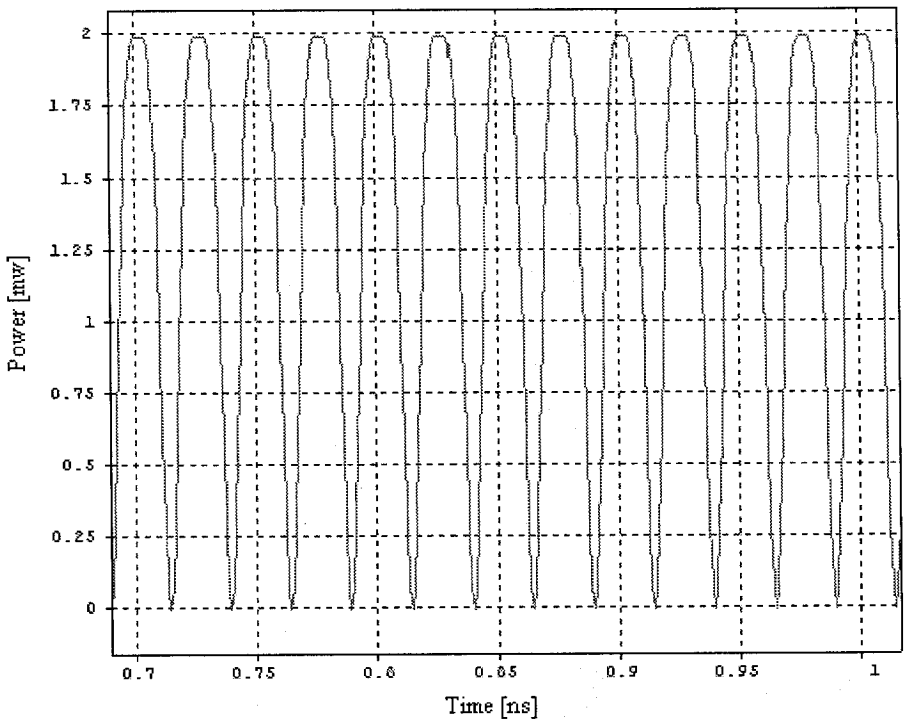

Figure 7: 66% duty cycle pulse carver at bit rate of 40 Gb/s.

The full width at half maximum (FWHM) of the pulse is 66%, and the peak to peak width is half the cycle period of the sinusoidal wave of driving voltage.

2.23 Spectral characteristics of 33% and 66% duty cycle RZ pulses

Figure 8 shows the optical spectrum of 33% RZ pulses without data modulation; its central carrier frequency is 194 THz, which is corresponding to the optical carrier of $\lambda = 1545.32$ nm.

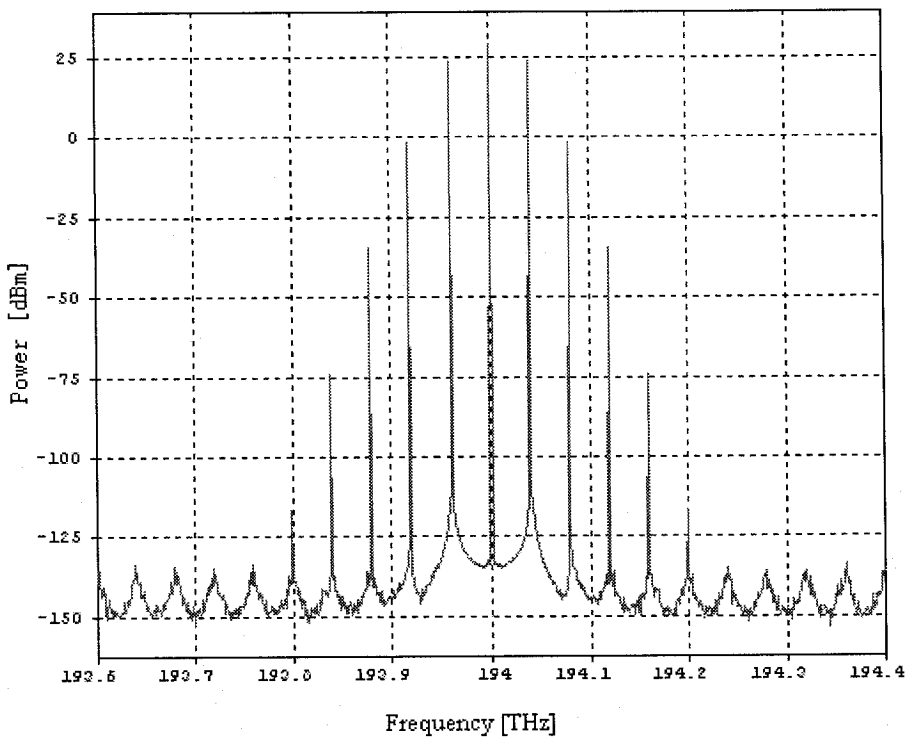

Figure 8: Optical spectrum of 33% RZ pulses without data modulation at bit rate of 40 Gb/s.

Figure 9 shows the optical spectrum of 66% RZ pulses without data modulation; its central carrier frequency is 194 THz, which is corresponding to the optical carrier $\lambda = 1545.32$ nm.

Comparing Figures 8 and 9, we can see that carrier frequency in the 66% RZ pulses is eliminated. Therefore, 66% pulses are also called carrier suppressed return zero (CSRZ) pulses.

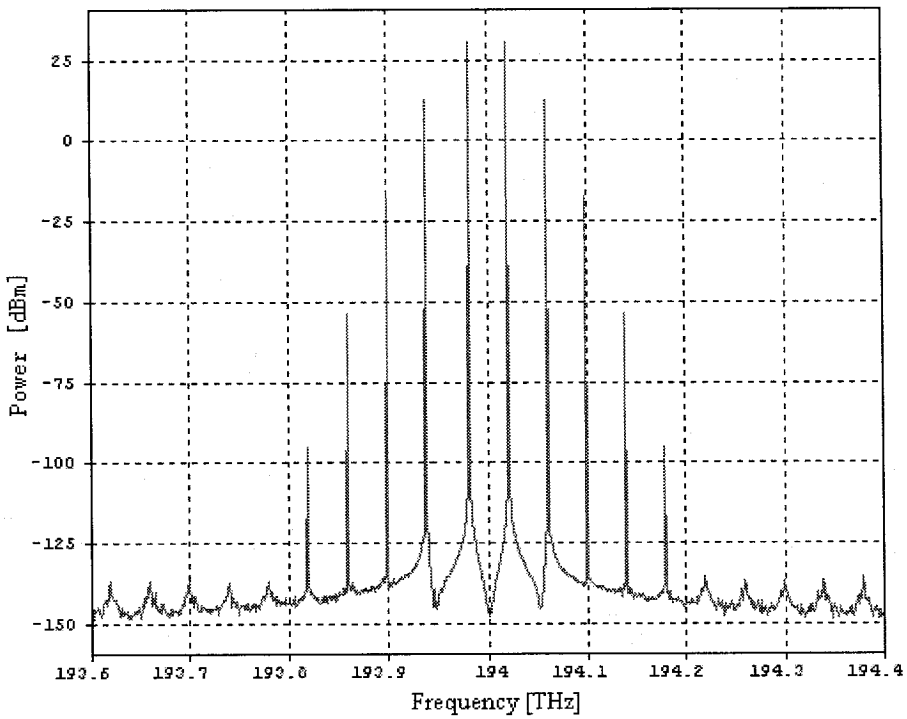

Figure 9: Optical spectrum of 66% RZ pulse without data modulation at bit rate of 40 Gb/s

With data modulation, both optical power spectra of 33% and 66% pulses become continues shown in Figures 10 and 11.

Comparing Figures 10 and 11, we can see that 66% pulse has compact optical spectrum and most power is condensed in the main lob. Investigation [44] concluded that CSRZ has a 3 dB enhancement in the maximum allowable fiber-launched power under fiber nonlinearity. Therefore, we only consider CSRZ pulses in the latter part of this thesis.

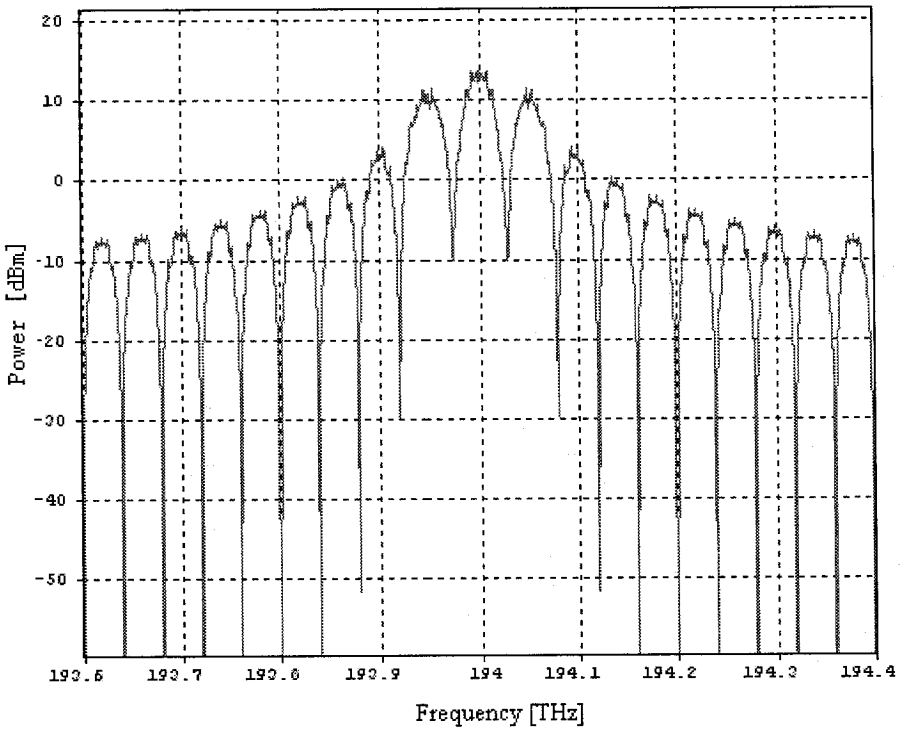

Figure 10: Optical spectrum of 33% RZ pulses with π-DPSK modulation at bit rate of 40 Gb/s.

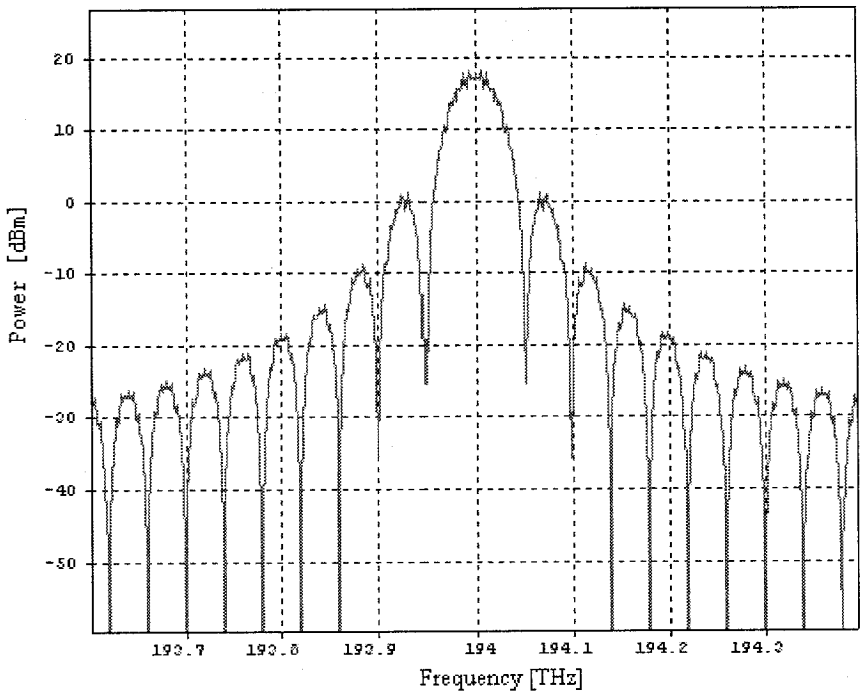

Figure 11: Optical spectrum of 66% RZ pulses with π-DPSK modulation at bit rate of 40 Gb/s.

2.3 Optical Mach-Zehnder delay interferometer (MZI)

Squared law photo diode detection is phase insensitive. We need phase to intensity conversion before optical detection to demodulate phase shift keying signal. Differential detection is a signal self reference technique to transfer phase to intensity; therefore we can use a general photo diode to convert the optical signal back into electronic form and recover the data transmitted through the light wave system.

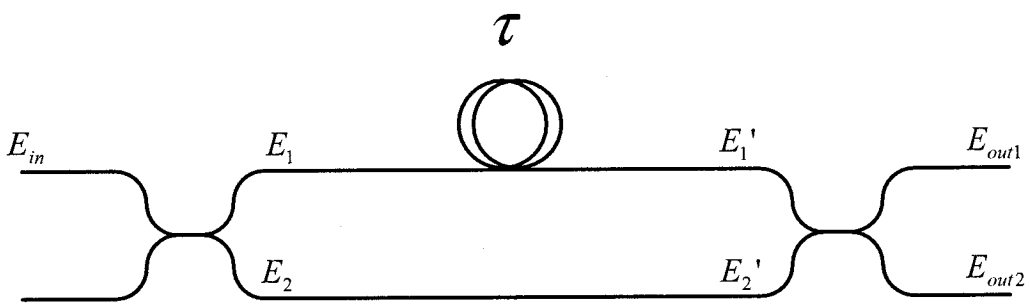

Figure 12: Optical March-Zehnder delay interferometer.

Figure 12 shows an all fiber optical March-Zehnder delay interferometer (MZI). E_{in} is electric field of input optical signal. E_1 and E_2 are outputs of first optical coupler. τ is time delay interval induced by a roll of optical fiber. E_1' is the output of the delay line, $E_2' = E_2$, and E_{out1} E_{out2} are outputs of the MZI.

An all-fiber optical Mach-Zehnder delay interferometer is constructed by connecting two fiber couplers in series with one arm making use of a delay line. The period of the delay line is one bit or several bits. The first 3 dB coupler splits the input signal into two parts, E_1 and E_2:

$$\begin{pmatrix} E_1 \\ E_2 \end{pmatrix} = \begin{pmatrix} \sqrt{\frac{1}{2}} & -j\sqrt{\frac{1}{2}} \\ -j\sqrt{\frac{1}{2}} & \sqrt{\frac{1}{2}} \end{pmatrix} \bullet \begin{pmatrix} E_{in} \\ 0 \end{pmatrix} \tag{2.9}$$

E_1' is the delayed version of $E_1, E_1' = E_1(t-\tau)$. The second 3 dB coupler combines E_1' and E_2', then E_{out1} and E_{out2} are given by

$$\begin{pmatrix} E_{out1} \\ E_{out2} \end{pmatrix} = \begin{pmatrix} \sqrt{\frac{1}{2}} & -j\sqrt{\frac{1}{2}} \\ -j\sqrt{\frac{1}{2}} & \sqrt{\frac{1}{2}} \end{pmatrix} \bullet \begin{pmatrix} E_1' \\ E_2 \end{pmatrix} \tag{2.10}$$

After arithmetic manipulation we have

$$E_{out1}(t) = \frac{1}{2}[E_{in}(t-\tau) - E_{in}(t)] \tag{2.11a}$$

$$E_{out2}(t) = \frac{-j}{2}[E_{in}(t-\tau) + E_{in}(t)] \tag{2.11b}$$

Without loss of generality, here we only consider one bit delay line, τ =1 bit period. Note the shape and power of successive pulses in phase modulated signal are constant. Supposed that $\Delta\theta_1$ and $\Delta\theta_2$ are of two successive pulses relative phases to the laser carrier, Equation (2.11) can be written as

$$E_{out1}(t) = \frac{1}{2}E_{pulse}\left[e^{j\Delta\theta_1} - e^{j\Delta\theta_2}\right] = -E_{pulse}\cos\frac{\Delta\theta_1 - \Delta\theta_2}{2}\exp\left(j\frac{\Delta\theta_1 + \Delta\theta_2}{2}\right) \tag{2.12a}$$

$$E_{out2}(t) = \frac{-j}{2}E_{pulse}\left[e^{j\Delta\theta_1} + e^{j\Delta\theta_2}\right] = jE_{pilse}\sin\frac{\Delta\theta_1 - \Delta\theta_2}{2}\exp\left(j\frac{\Delta\theta_1 + \Delta\theta_2}{2}\right) \tag{2.12b}$$

2.4 Balanced photodiode detection

An ideal photodiode can be thought as a squared law component with a low pass filter,

$$\text{i.e. } I_{diode} = R|E_{in}|^2, \tag{2.13}$$

where I_{diode} is the photocurrent of the diode, and R is the responsivity of the photodiode.

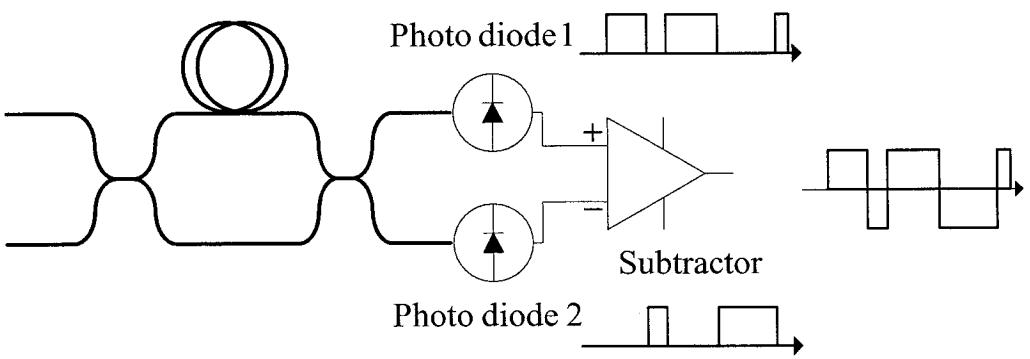

Figure 13: Balanced photodiode detection.

Figure 13 shows the balanced photodiode detection. Two photodiode are connected to each arm of a MZI. Substituting Equation (2.12) to Equation (2.13), we get

$$I_{diode1} = R|E_{out1}(t)|^2 = RP_{pulse}\left|\cos\frac{\Delta\theta_1 - \Delta\theta_2}{2}\right|^2 \tag{2.14a}$$

$$I_{diode2} = R|E_{out2}(t)|^2 = RP_{pulse}\left|\sin\frac{\Delta\theta_1 - \Delta\theta_2}{2}\right|^2 \tag{2.14b}$$

where P_{pulse} is the power of optical pulse.

After the subtracter, we get

$$I_{subtractor} = RP_{pulse}\left(\left|\cos\left(\frac{\Delta\theta_1 - \Delta\theta_2}{2}\right)\right|^2 - \left|\sin\left(\frac{\Delta\theta_1 - \Delta\theta_2}{2}\right)\right|^2\right) \tag{2.14c}$$

We can see based on Equation (2.14) that phase difference $\Delta\theta_1 - \Delta\theta_2$ of successive

bits can be manifested through the photocurrents of I_{diode1}, I_{diode2} and $I_{subtractor}$.

Sometimes, we called the cosine arm as the constructive port and the sine arm as the destructive port, because the cosine arm gives a logic '1' while the sine arm gives a logic '0' when the successive bits are inphase.

Balanced photodiode detection gives a 3 dB SNR improvement than the single arm detection.

Chapter 3

System modeling and electronic precoder

In this chapter, we present four models of differential phase modulation schemes based on the phase constellations carried by the optical line code, and they are π-DPSK, $\pi/2$-DPSK, DQPSK, Offset-DQPSK. In π-DPSK model, the phase difference $\Delta\phi$ between two successive bits is in the set $\{0,\pi\}$. In $\pi/2$-DPSK model, $\Delta\phi$ is in the set $\{-\pi/2,\pi/2\}$. In DQPSK model, $\Delta\phi$ is in the set $\{-\pi/2,0,\pi/2,\pi\}$. In Offset-DQPSK, $\Delta\phi$ is in the set $\{-\pi/2,0,\pi/2\}$.

All these models were verified in Optsim 4.0. Appendix B gives the simulation setups for these models.

3.1 π-DPSK

3.11 System modeling for π-DPSK

A π-DPSK system model is represented schematically in Figure 14. The output of a laser is modulated with a 66% pulse carver. The RZ pulse is then sent to a MZM modulator driven by a pseudorandom bit sequence (PRBS). An electronic precoder

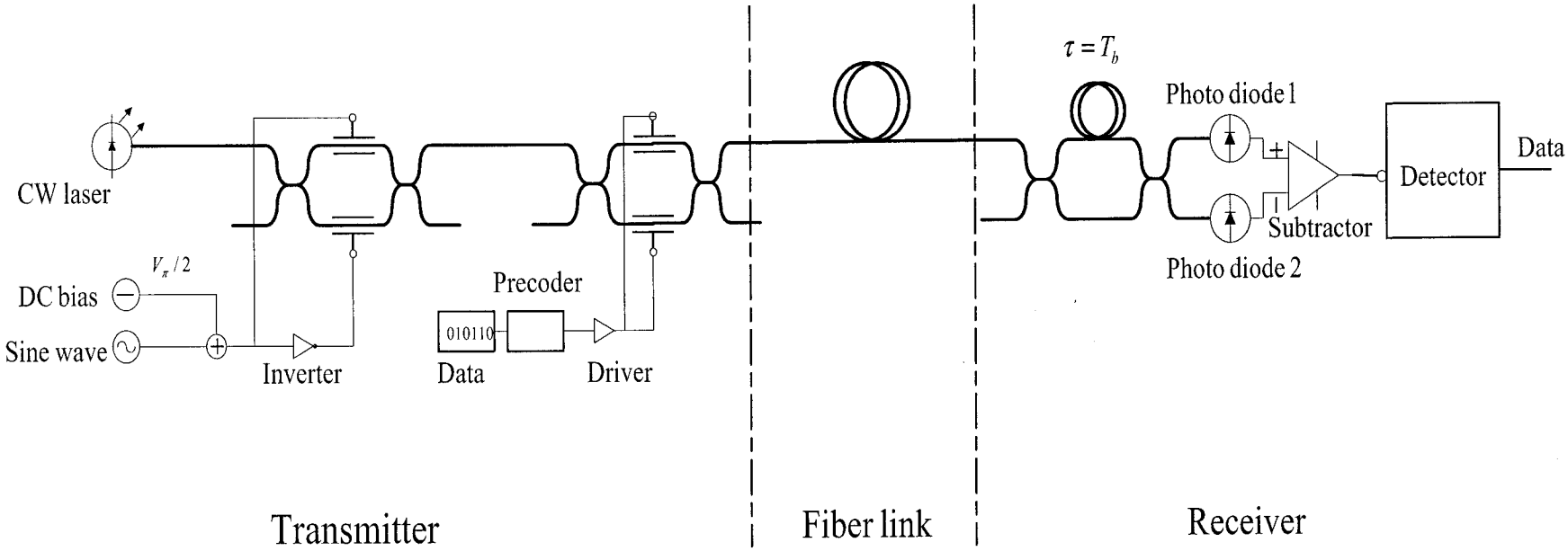

Figure 14 : Schematic for π – DPSK system model.

between PRBS and MZM is required to counteract the logic of whole transmission system. The frequency of the sine wave in the pulse carver is half of the bit rates of the PRBS. The sine wave and the PRBS should be synchronized; and it means that the RZ pulse and phase modulated pulse must be kept in the same period. The modulated signal passes through a fiber link. At the output of the fiber link, we employ an MZI and two photodiodes which work as a balanced signal detection.

In π-DPSK system, each transmitted symbol conveys one bit information. The data information is encoded in $\Delta\phi$, which is the phase difference between successive symbols. Figure 15 shows the line code of π-DPSK system. We can see $\Delta\phi \in (0,\pi)$.

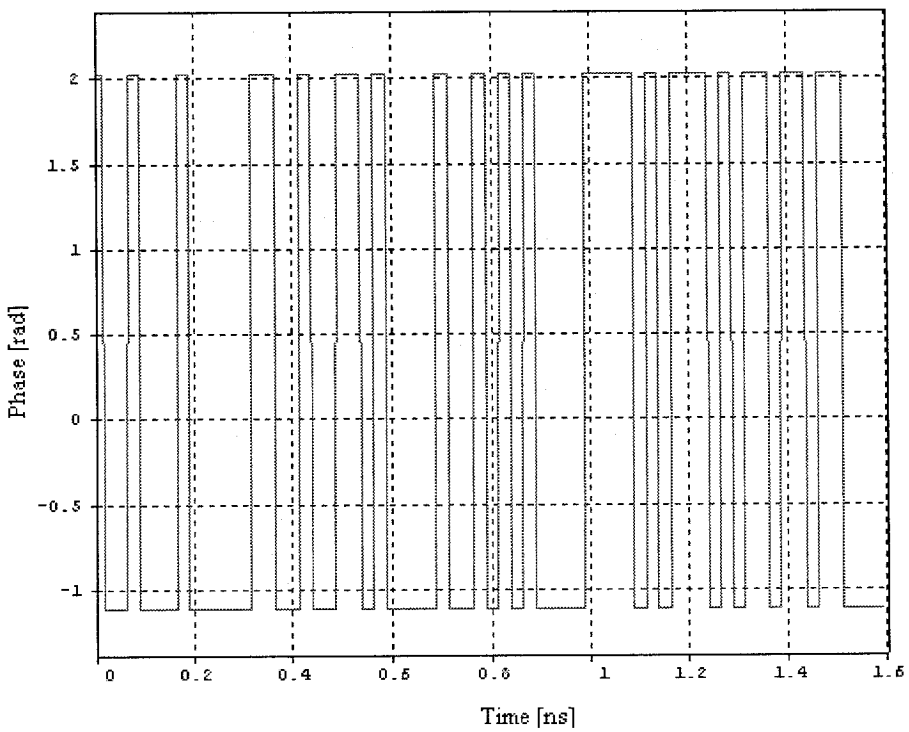

Figure 15: Line code of π-DPSK, where $\Delta\phi \in (0,\pi)$.

Figure 16 shows the external modulator used in π-DPSK transmitter. Two arms of

the MZM have equal electronic driving voltage. The peak to peak of driving voltage is V_π that means $\theta_1 = \theta_2 \in (0,\pi)$, where θ_1 and θ_2 are phase changes of two arms. In this setup, the MZM works as a phase modulator, Equation (2.6) can be written

$$E_{out1} = E_{out2} = E_{in} \exp\left(j\frac{\theta_1 + \theta_2}{2} \right). \tag{3.1}$$

We see that two output ports of the MZM have equal electronic field.

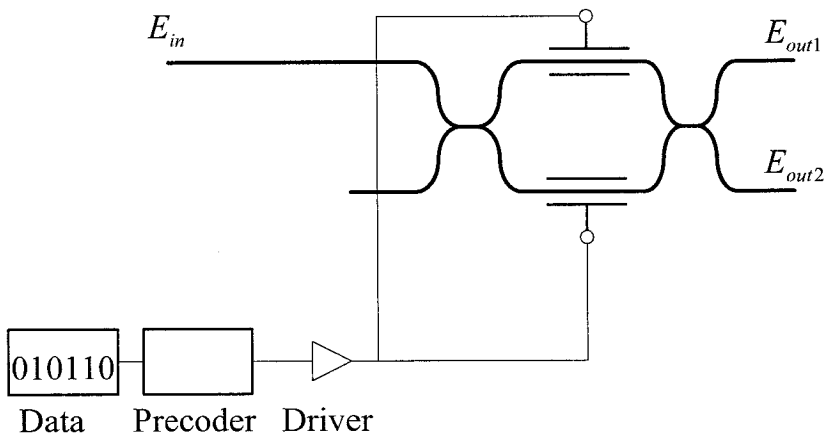

Figure 16: π-DPSK phase modulator.

In π-DPSK receiver, modulated signal passed into an optical delay-line Mach-Zehnder interferometer (MZI), see Figure 17. We assume that the interferometer's two branches have correctly one bit delay, τ=1 bit period of T_b, so Equation (2.14) can be written

$$I_{diode1} = R\left|E_{out1}(t)\right|^2 = RP_{pulse}\left|\cos\frac{\Delta\phi}{2}\right|^2 \tag{3.2a}$$

$$I_{diode2} = R\left|E_{out2}(t)\right|^2 = RP_{pulse}\left|\sin\frac{\Delta\phi}{2}\right|^2 \tag{3.2b}$$

where $\Delta\phi \in (0, \pi)$ is phase difference between successive bit sequences.

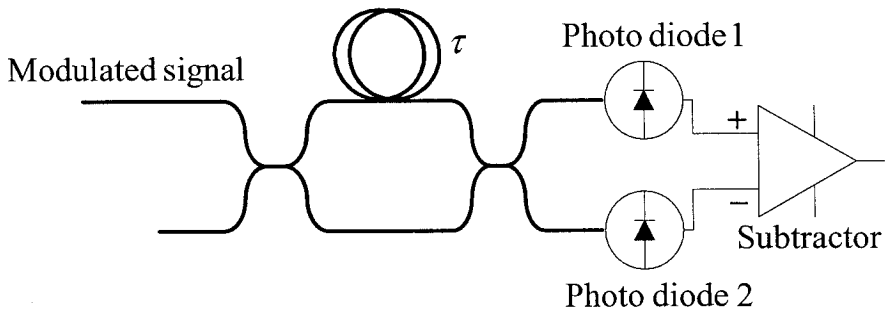

Figure 17: π-**DPSK receiver**.

3.12 Electronic precoder for π-DPSK

The differential detector operates by multiplying the received signal by its delayed version. Without loss of generality, we use the sine arm as the detection output defined in Equation (2.14). The logic of the received signal is '0' when two successive bits have no phase difference and '1' when π difference is presented.

Table 1 Truth table of π-DPSK without precoder.

$D_{in}(t)$	$D_{in}(t-T_b)$	$\Delta\theta$	$\Delta\theta(t)-\Delta\theta(t-T_b)$	$\left\|\sin\left(\frac{\Delta\theta(t)-\Delta\theta(t-T_b)}{2}\right)\right\|^2$
0	0	0		
1	0	π	π	1
1	1	π	0	0
0	1	0	$-\pi$	1
1	0	π	π	1
0	1	0	$-\pi$	1

In order to disclose the transmission logic of π-DPSK, Table 1 is used to depict the system without precoder. Table 1 is the truth table of π-DPSK without precoder, where $D_{in}(t)$ is data of PRBS to be encoded and transmitted through the lightwave system, $D_{in}(t-T_b)$ is one bit delay of $D_{in}(t)$, $\Delta\theta$ is phase shift keying corresponding to $D_{in}(t)$, $\Delta\theta(t)-\Delta\theta(t-T_b)$ is phase difference of successive bits at receiver, $\left|\sin\left(\frac{\Delta\theta(t)-\Delta\theta(t-T_b)}{2}\right)\right|^2$ is the output of the sine arm of the MZI defined in Equation (3.2). According to Table 1, we concluded that

$$D_{out} = \overline{D_{in}(t)}D_{in}(t-T_b)+D_{in}(t)\overline{D_{in}(t-T_b)} \tag{3.3}$$

This is a logic equation where D_{out} is the data of π-DPSK output, a bar over a symbol means NOT logic.

In order to give a correct data corresponding to the transmitted data, we need an electronic precoder in the transmitter. Figure 18 shows the logic structure of electronic precoder for π-DPSK.

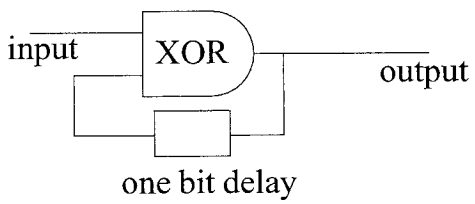

Figure 18: Electronic precoder for π-DPSK.

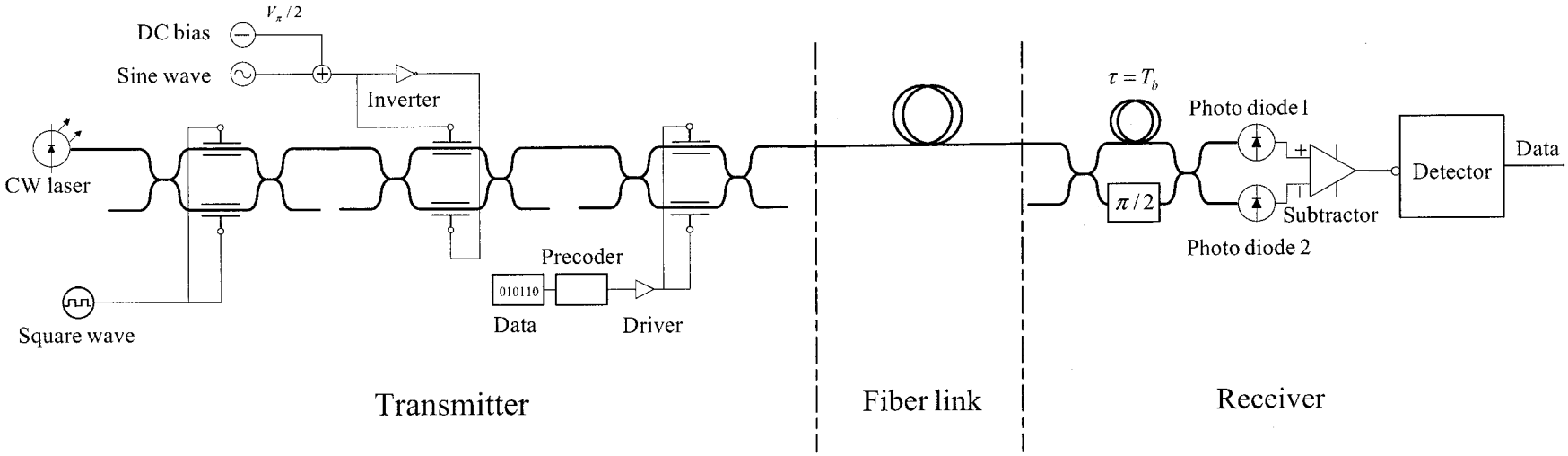

Figure 19 : Schematic for $\pi / 2$ - DPSK system model

3.2 $\pi/2$-DPSK

3.21 System modeling for $\pi/2$-DPSK

Figure 19 shows the $\pi/2$-DPSK system model. The output of a laser is modulated alternatively with a $\pi/2$ phase shift. This process generates a $\pi/2$ alternate phase pulses train. One method to generate a $\pi/2$ alternate phase shift pulses train is by push-push driving a MZM with a square wave. The alternate phase shift pulses train is modulated with a 66% pulse carver. The RZ pulses are sent to a MZM modulator driven by a pseudorandom bit sequence (PRBS). An electronic precoder between PRBS and MZM is required to counteract the logic of whole transmission system. Both frequencies of the square wave in the generator of $\pi/2$ alternate phase shift pulses train and the sine wave in the pulse carver are half of the bit rates of the PRBS. The square wave, sine wave and the PRBS should be synchronized, which means that the $\pi/2$ alternate phase pulse, RZ pulse and phase modulated pulse must be kept in the same period. The modulated signal passes through a fiber link. At the output of the fiber link, we employed an MZI which one arm is $\pi/2$ phase shifted. After the MZI, two photodiodes are also used to work as balanced signal detection.

In $\pi/2$-DPSK system, each transmitted symbol conveys one bit information. The data information is encoded in $\Delta\phi$, which is the phase difference between successive symbols. Figure 20 shows the line code of $\pi/2$-DPSK system. We can see $\Delta\phi \in (-\pi/2, \pi/2)$.

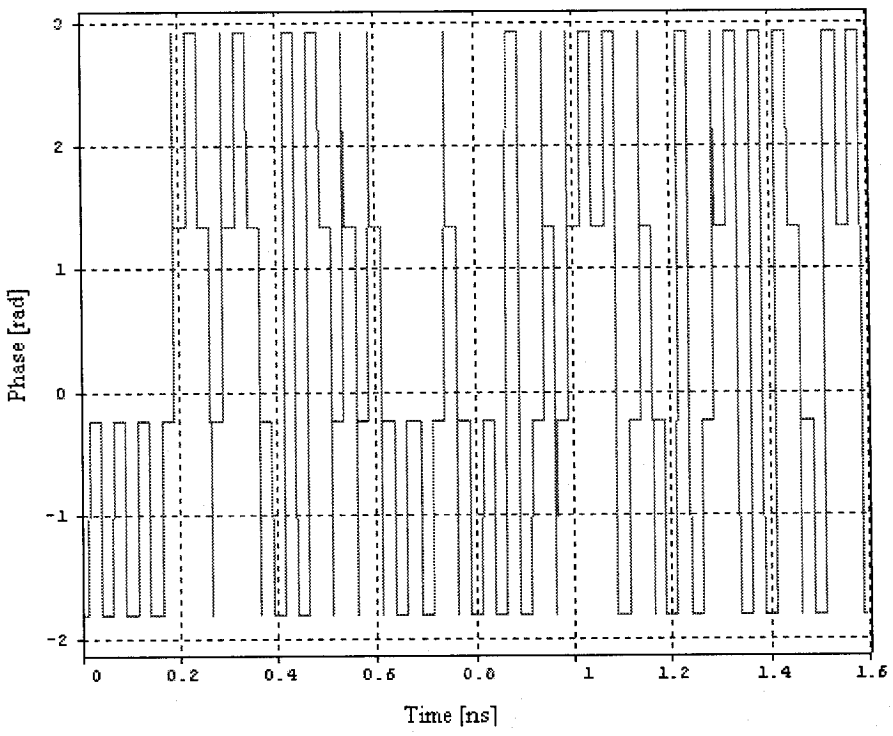

Figuer 20: Line code of DPSK, $\Delta\phi \in (-\pi/2, \pi/2)$

The optical $\pi/2$ -DPSK transmitter is similar to the DPSK transmitter, and the main difference is that $\pi/2$ -DPSK requires an optical pulse generator to produce a pulse

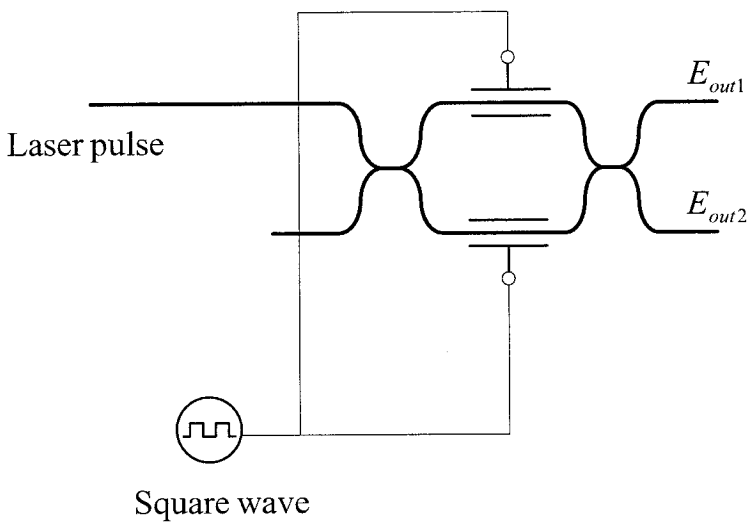

Figure 21: Generator of $\pi/2$ alternate phase shift pulse train.

train with $\pi/2$ alternate phase shift. Figure 21 shows the generator of $\pi/2$ alternate phase shift pulses train.

A MZM is driven by a square wave voltage. The peak to peak value of the square wave is $V_\pi/2$. As a result, the phase difference between any two adjacent pulses is $\pi/2$ and $-\pi/2$. Figure 22 shows the $\pi/2$ alternate phase shift pulse train.

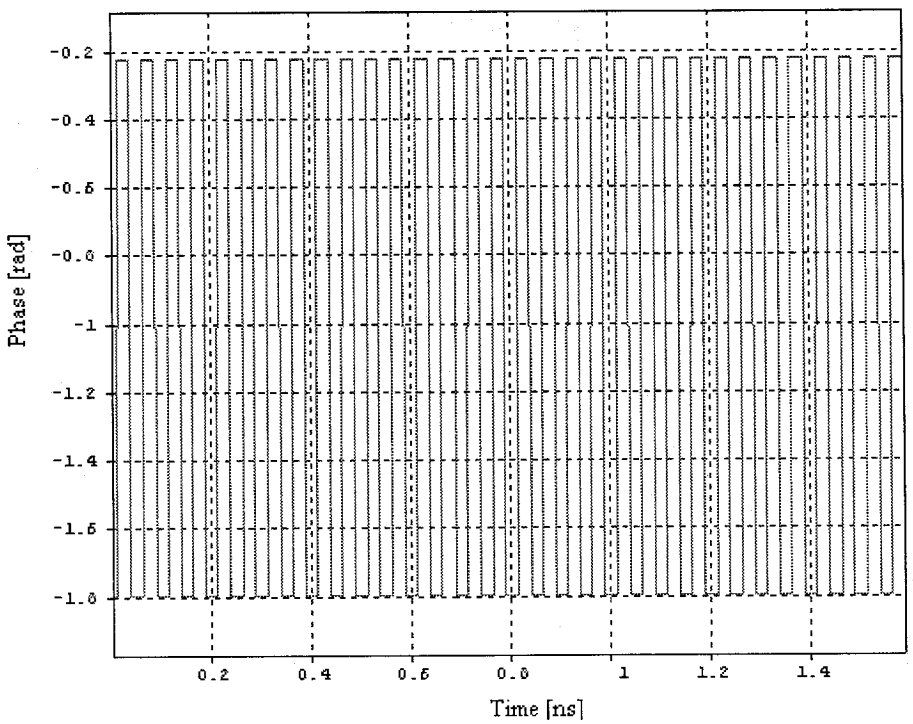

Figure 22: $\pi/2$ alternate phase shift pulse train.

Figure 23 shows the receiver of $\pi/2$-DPSK. A phase modulator driven by $V_\pi/2$ DC voltage is used in the spare arm of the MZI. It gives a constant $\pi/2$ phase shift. The interferometer's two branches have correctly one bit time delay, which τ=1 bit period. In this condition, Equation (2.14) can be written

$$I_{diode1} = RP_{pulse}\left|\cos\left(\frac{\Delta\theta}{2}+\frac{\pi}{4}\right)\right|^2 \qquad (3.4a)$$

$$I_{diode2} = RP_{pulse}\left|\sin\left(\frac{\Delta\theta}{2}+\frac{\pi}{4}\right)\right|^2 \qquad (3.4b)$$

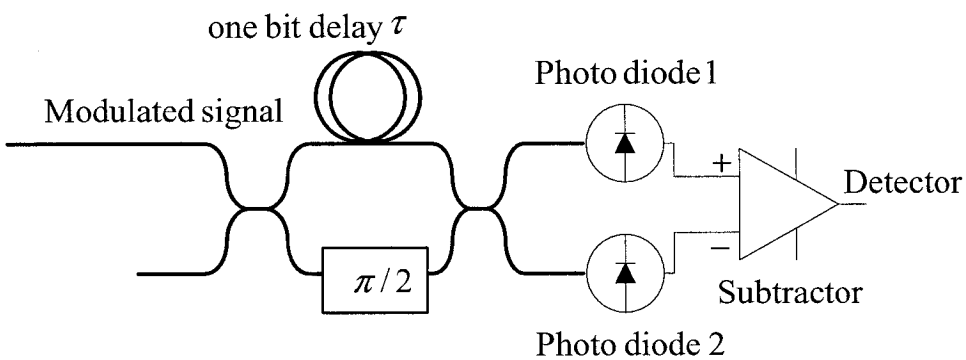

Figure 23: Optical receiver for $\pi/2$-DPSK.

3.22 Electronic precoder for $\pi/2$-DPSK

Without loss of generality, we use the cosine arm as the detection output of $\pi/2$-DPSK. In order to disclose the transmission logic of $\pi/2$-DPSK, Table 2 is used to depict the system without precoder. Notice that the clock of the alternative $\pi/2$ phase shift is involved in the modulation.

Table 2 Truth table of $\pi/2$-DPSK transmission

(C=$\pi/2$ corresponding to logic '1')

Hex	A	B	C	$\Delta\theta$	$\Delta\theta-\theta_{pulse}$	$\Delta\theta(t)-\Delta\theta(t-T_b)$	D_{out}
1	0		$\pi/2$	0	$-\pi/2$		
4	1	0	0	π	π	$\pi 3/2$	1
3	0	1	$\pi/2$	0	$-\pi/2$	$-\pi 3/2$	0
4	1	0	0	π	π	$\pi 3/2$	1
7	1	1	$\pi/2$	π	$\pi/2$	$-\pi/2$	1
2	0	1	0	0	0	$-\pi/2$	1
1	0	0	$\pi/2$	0	$-\pi/2$	$-\pi/2$	1
0	0	0	0	0	0	$\pi/2$	0
5	1	0	$\pi/2$	π	$\pi/2$	$\pi/2$	0
6	1	1	0	π	π	$\pi/2$	0
3	0	1	$\pi/2$	0	$-\pi/2$	$-\pi 3/2$	0

Table 2 is the truth table of $\pi/2$-DPSK without precoder. Where A= $D_{in}(t)$ is data of PRBS to be encoded and transmitted through the lightwave system, B=$D_{in}(t-T_b)$ is one bit delay of $D_{in}(t)$, C=θ_{pulse} is alternative $\pi/2$ phase shift, $\Delta\theta$ phase shift keying corresponding to $D_{in}(t)$, $\Delta\theta-\theta_{pulse}$ is combined phase shift of data and alternative $\pi/2$ shift, $\Delta\theta(t)-\Delta\theta(t-T_b)$ is phase difference of successive bits at receiver, $D_{out}=\left|\cos\left(\frac{\Delta\theta(t)-\Delta\theta(t-T_b)}{2}+\frac{\pi}{4}\right)\right|^2$ is the output of the

cosine arm of the MZI defined in Equation (3.4). According to Table 2, we concluded that

$$D_{out} = \overline{\overline{A}BC} + A\overline{B}\overline{C} + ABC + \overline{A}B\overline{C} \qquad (3.5)$$

This is a logic equation where D_{out} is the data of $\pi/2$-DPSK output, a bar over a symbol means NOT logic. In order to give a correct data corresponding to the transmitted data, we need an electronic precoder in the transmitter. Figure 24 shows the logic structure of an electronic precoder for $\pi/2$-DPSK.

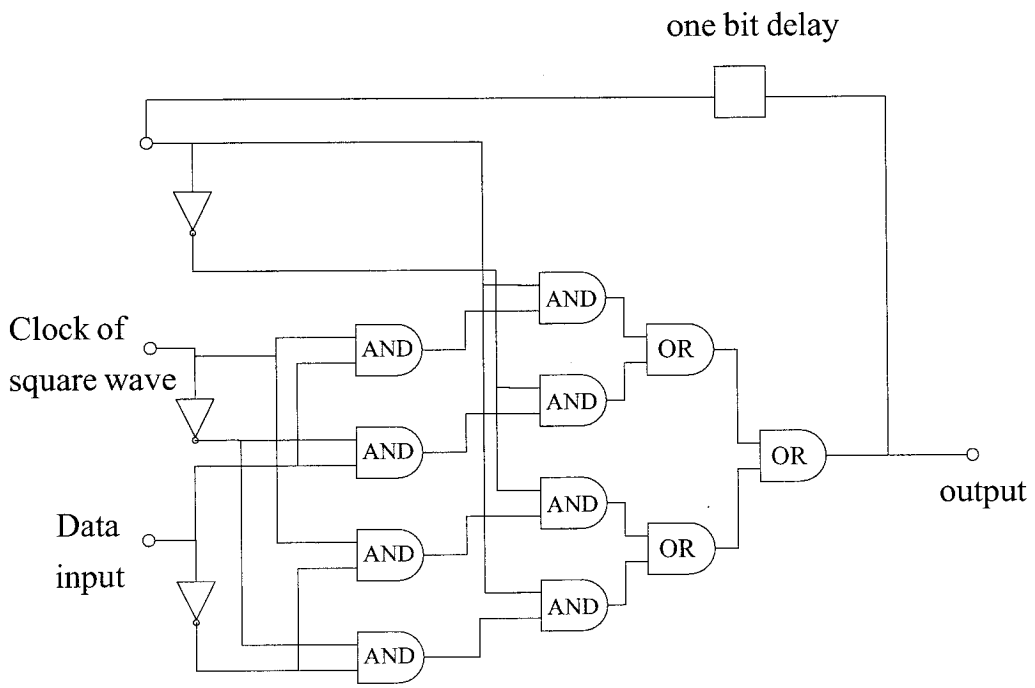

Figure 24: Schematic of electronic precoder for $\pi/2$-DPSK.

Figures 25 and 26 show the simulation results of precoder for $\pi/2$-DPSK. The PRBS polynomial degree of data source are 2^9 and 2^{10} respectively. We can see the data of input at transmitter match the data of output at receiver correctly.

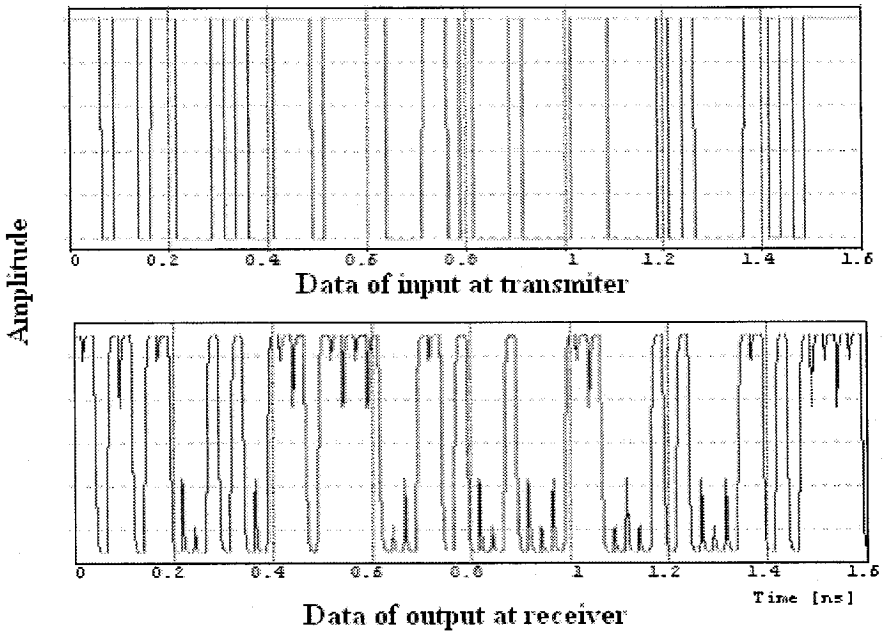

Figure 25: Simulated result of $\pi/2$-DPSK precoder at 2^9 PRBS.

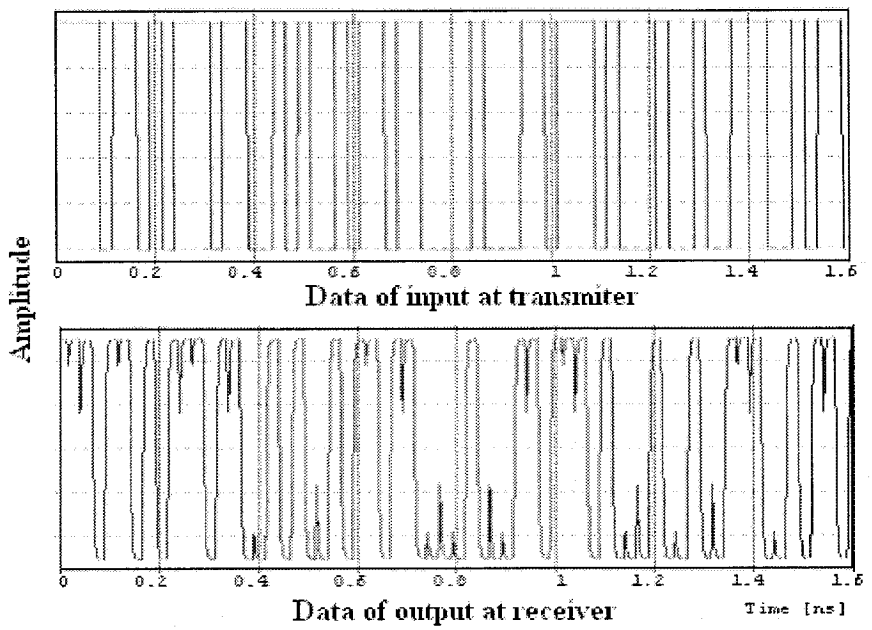

Figure 26: Simulated result of $\pi/2$-DPSK precoder at 2^{10} PRBS.

3.3 DQPSK

3.31 System modeling for DQPSK

Figure 27 shows the DQPSK system model. The output of a laser is modulated with a 66% pulse carver. The RZ pulse is sent to a MZM modulator driven by two pseudorandom bit sequence (PRBS). The bit rates of two PRBSs are half of the transmission bit rates. An electronic precoder between PRBS and MZM is required to counteract the logic of whole transmission system. The frequency of the sine wave in the pulse carver is equal to the bit rates of the PRBS. The sine wave and two PRBS should be synchronized which it means that the RZ pulse and phase modulated pulse must be kept in the same period. The modulated signal passes through a fiber link. At the output of the fiber link, we split the signal into two branches. Two MZIs and two balanced photodiode detectors are employed. Each MZI has its own phase modulator in its spare arm; one phase modulator gives a constant $\pi/4$ phase shift, and the other one gives a constant $-\pi/4$ phase shift.

DQPSK has twice the bandwidth efficiency of BPSK, since two bits are transmitted in a single modulation symbol. The data information is encoded in $\Delta\phi$, which is the phase difference between successive symbols. Figure 28 shows the line code of DQPSK. We can see $\Delta\phi \in \{-\pi/2, 0, \pi/2, \pi\}$.

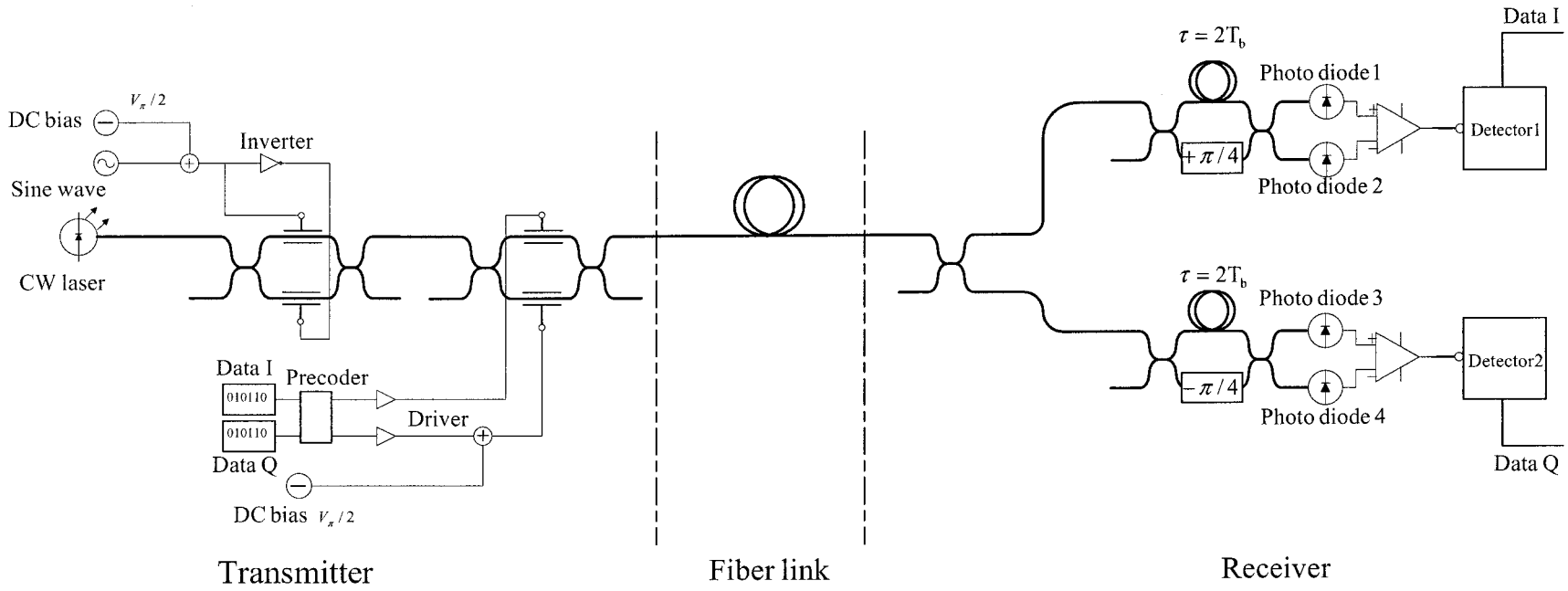

Figure 27 : Schematic for DQPSK system model.

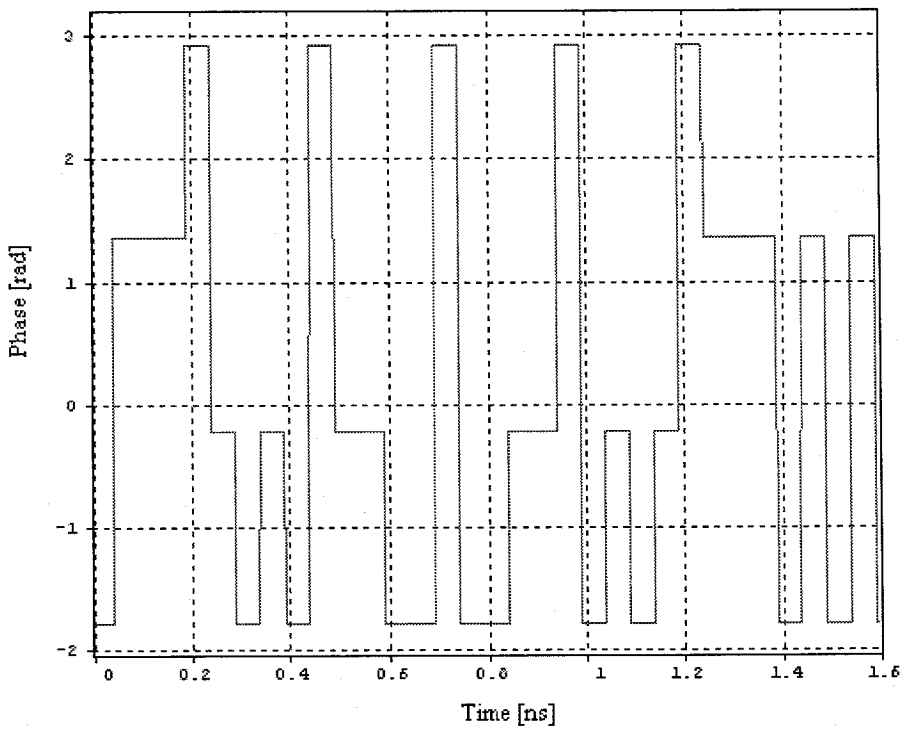

Figure 28: Line code of DQPSK with $\Delta\phi \in \{-\pi/2, 0, \pi/2, \pi\}$.

A convenient orthogonal realization of DQPSK waveform is achieved by amplitude modulating the in-phase and quadrature data streams onto two carriers which have $\pi/2$ phase difference. Figure 29 depicts the structure of an optical DQPSK modulator.

A MZM modulator is driven by two branches of information data. One arm of the modulator is biased by $V_\pi/2$ DC voltage, generating a $\pi/2$ constant phase shift. In this condition Equation (2.6) can be written

$$E_{out} = E_{in} \sin\left(\frac{\theta_1 - \theta_2}{2} - \frac{\pi}{4}\right) \exp\left(j\frac{\theta_1 + \theta_2}{2} + \frac{\pi}{4}\right) \tag{3.6}$$

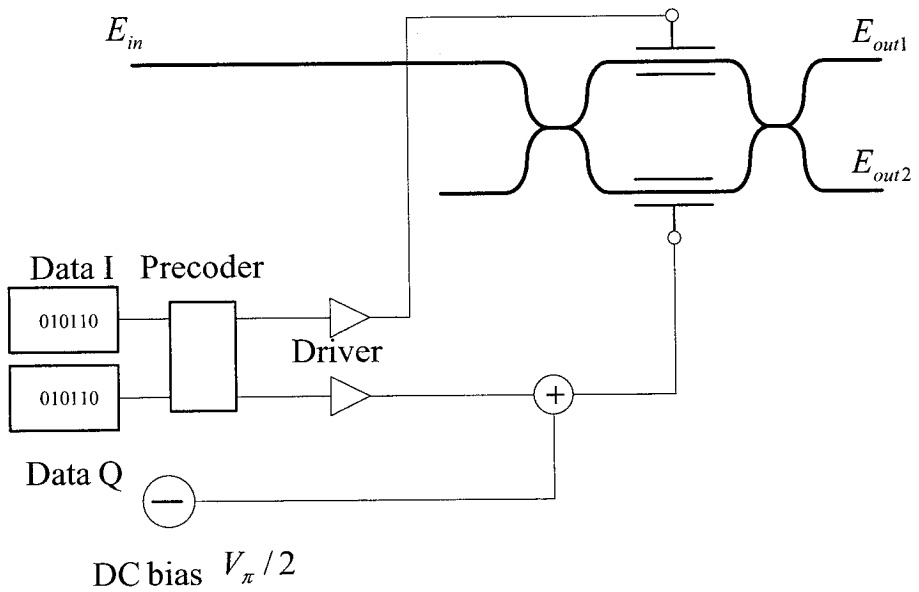

Figure 29: Schematic of DQPSK modulator.

Where E_{in} is electric field of laser carrier, θ_1 and θ_2 are two phase shifts corresponding to inphase and quadrature data and both θ_1 and θ_2 are belong to the set of $(0,\pi)$. Here we only account one output arm for simplicity. We can see that the exact phase change of E_{out} depends on not only the exponential term but also the sine term of Equation (3.6). Figure 30 shows the phase constellation of DQPSK

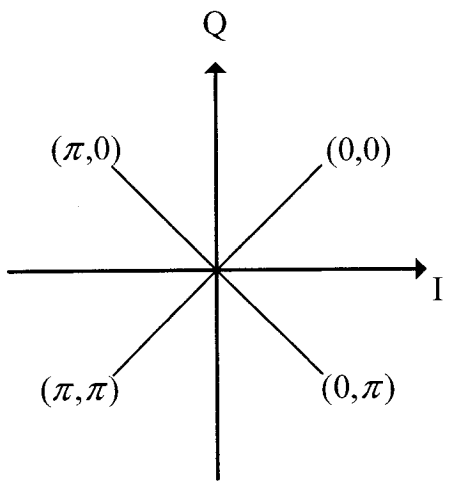

$$\sin\left(\frac{\theta_1-\theta_2}{2}-\frac{\pi}{4}\right)\exp\left(j\frac{\theta_1+\theta_2}{2}+\frac{\pi}{4}\right)$$

Figure 30: Phase constellation of DQPSK signal.

signal.

To demodulate DQPSK signal, two branches of delay interferometer are required, shown in Figure 31.

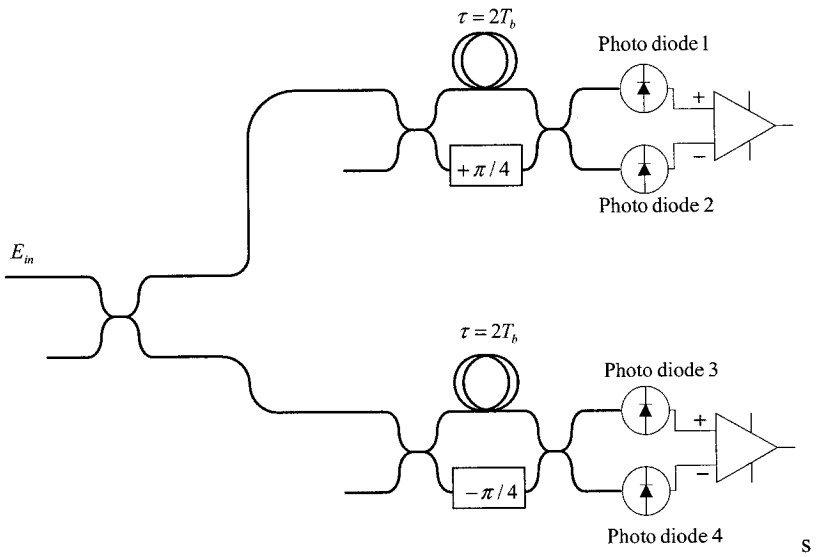

Figure 31: Schematic of DQPSK receiver.

Two branches have same structure except that one branch has $+\pi/4$ phase shift while the other has $-\pi/4$ phase shift. In this condition, Equation (2.14) can be written as

$$I_{subtractor1} = RP_{pulse}\left(\left|\sin\left(\frac{\Delta\theta_1 - \Delta\theta_2}{2} + \frac{\pi}{8}\right)\right|^2 - \left|\cos\left(\frac{\Delta\theta_1 - \Delta\theta_2}{2} + \frac{\pi}{8}\right)\right|^2\right) \quad (3.7a)$$

$$I_{subtractor2} = RP_{pulse}\left(\left|\sin\left(\frac{\Delta\theta_1 - \Delta\theta_2}{2} - \frac{\pi}{8}\right)\right|^2 - \left|\cos\left(\frac{\Delta\theta_1 - \Delta\theta_2}{2} - \frac{\pi}{8}\right)\right|^2\right) \quad (3.7b)$$

3.32 Electronic precoder for DQPSK

In order to disclose the transmission logic of DQPSK, Table 3 is used to depict the

system without precoder.

Table 3 is the truth table of DQPSK without precoder, Where A= $D_{in1}(t)$ and B= $D_{in2}(t)$ are data of two PRBSs to be transmitted through the lightwave system, C= $D_{in1}(t-2T_b)$ and D= $D_{in2}(t-2T_b)$ are one bit delayed version of $D_{in1}(t)$ and $D_{in2}(t)$, $\Delta\phi = \theta_1 - \theta_2$ is phase shift keying corresponding to Equation (3.6), $\Delta\theta(t) - \Delta\theta(t-T_b)$ is phase difference of successive bits at receiver, I= $I_{subtractor1}$ and Q= $I_{subtractor2}$ are the outputs DQPSK demodulator defined in Equation (3.7). According to Table 3, we concluded that

$$D_{out1} = \overline{A}\overline{B}D + A\overline{B}\overline{D} + \overline{A}BC + A\overline{B}\overline{C} \qquad (3.8a)$$

$$D_{out2} = \overline{A}\overline{B}C + ABC + \overline{A}B\overline{D} + A\overline{B}D \qquad (3.8b)$$

This is a logic equation where D_{out1} and D_{out2} are the data of DQPSK output, a bar over a symbol means NOT logic. This result is consistent with [40].

Table 3. Truth table of DQPSK transmission

(0.3827 corresponding logic '0', 0.9239 corresponding to logic '1')

Hex	A	B	C	D	$\Delta\phi$	$\Delta\theta(t)-\Delta\theta(t-T_b)$	I	Q
0	0	0	0	0	$\pi/4$			
4	0	1	0	0	$-\pi/4$	$-\pi/2$	0.9239	0.3827
9	1	0	0	1	$3\pi/4$	π	0.9239	0.9239
E	1	1	1	0	$5\pi/4$	$\pi/2$	0.3827	0.9239
3	0	0	1	1	$\pi/4$	$-\pi$	0.9239	0.9239
8	1	0	0	0	$3\pi/4$	$\pi/2$	0.3827	0.9239
6	0	1	1	0	$-\pi/4$	$-\pi$	0.9239	0.9239
1	0	0	0	1	$\pi/4$	$\pi/2$	0.3827	0.9239
8	1	0	0	0	$3\pi/4$	$\pi/2$	0.3827	0.9239
2	0	0	1	0	$\pi/4$	$-\pi/2$	0.9239	0.3827
C	1	1	0	0	$5\pi/4$	π	0.9239	0.9239
7	0	1	1	1	$-\pi/4$	$-3\pi/2$	0.3827	0.9239
D	1	1	0	1	$5\pi/4$	$3\pi/2$	0.9239	0.3827
B	1	0	1	1	$3\pi/4$	$-\pi/2$	0.9239	0.3827
A	1	0	1	0	$3\pi/4$	0	0.3827	0.3827
6	0	1	1	0	$-\pi/4$	$-\pi$	0.9239	0.9239
5	0	1	0	1	$-\pi/4$	0	0.3827	0.3827
13	1	1	0	1	$5\pi/4$	$3\pi/2$	0.9239	0.3827
F	1	1	1	1	$5\pi/4$	0	0.3827	0.3827

In order to give a correct data corresponding to the transmitted data, we need an electronic precoder in the transmitter. Figure 32 shows the logic structure of electronic precoder for DQPSK system.

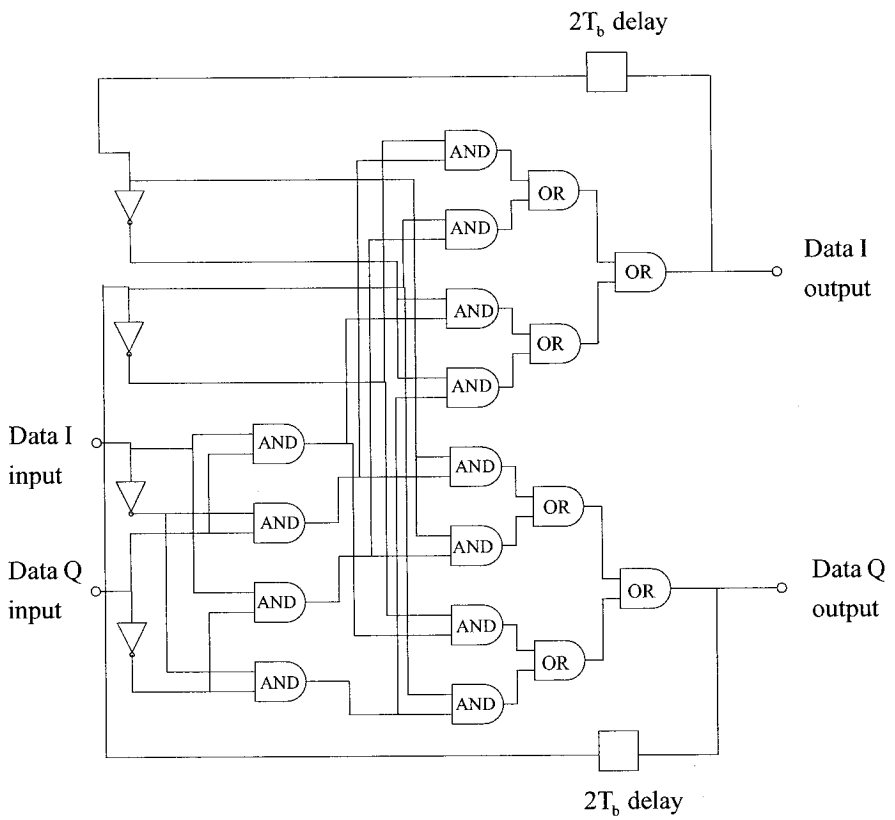

Figure 32: Schematic of electronic precoder for DQPSK.

Figures 33 and 34 show the simulated results of precoder for DQPSK, The polynomial degree of PRBS are 2^9 and 2^{10} respectively. We can see the data of input at transmitter match the data of output at receiver correctly.

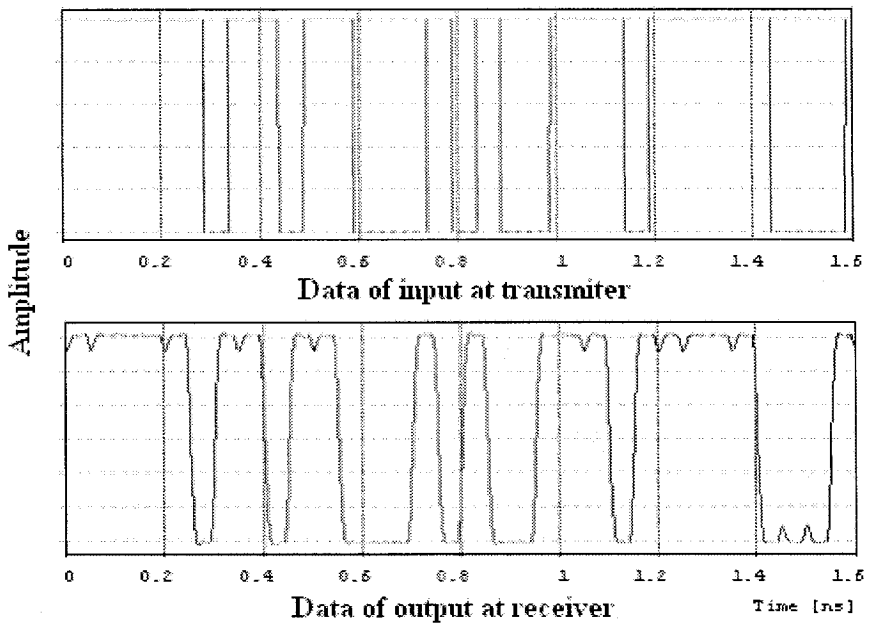

Figure 33: Simulated result of DQPSK precoder at 2^{10} PRBS.

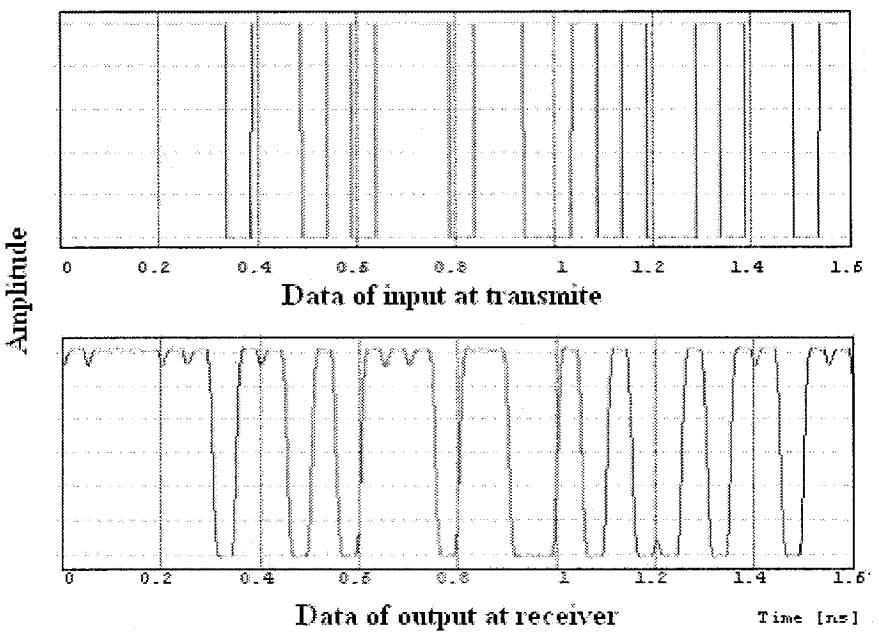

Figure 34: Simulated result of DQPSK precoder at 2^{10} PRBS.

3.4 Offset-DQPSK

3.41 System modeling for Offset-DQPSK

Figure 35 shows the Offset-DQPSK system model. Offset-DQPSK is considered to be an improvement over DQPSK from the view point of phase transitions. DQPSK presents a phase value of $\Delta\phi \in \{-\pi/2, 0, \pi/2, \pi\}$. This means that, in DQPSK signal, the transitions of the symbols in the two channels can occur at the same time. These simultaneous transitions create fluctuations of the signal envelope which becomes transiently zero. This can be an important source of performance degradation for systems with nonlinearity in the transmission link. To diminish the effect of the envelope fluctuations, one solution is to delay the quadrature channel signal by one bit duration from the inphase channel signal. The signal obtained by this operation is called Offset QPSK. The Offset QPSK signal does not allow a simultaneous change of the inphase and the quadrature signals, and therefore, the possibility of a phase change by π is eliminated.

In Offset-DQPSK system, information data is encoded in $\Delta\phi$, which is the phase difference between successive symbols. Figure 36 shows the line code of Offset-DQPSK. We can see $\Delta\phi \in \{-\pi/2, 0, \pi/2\}$, and the symbol period is half of DQPSK.

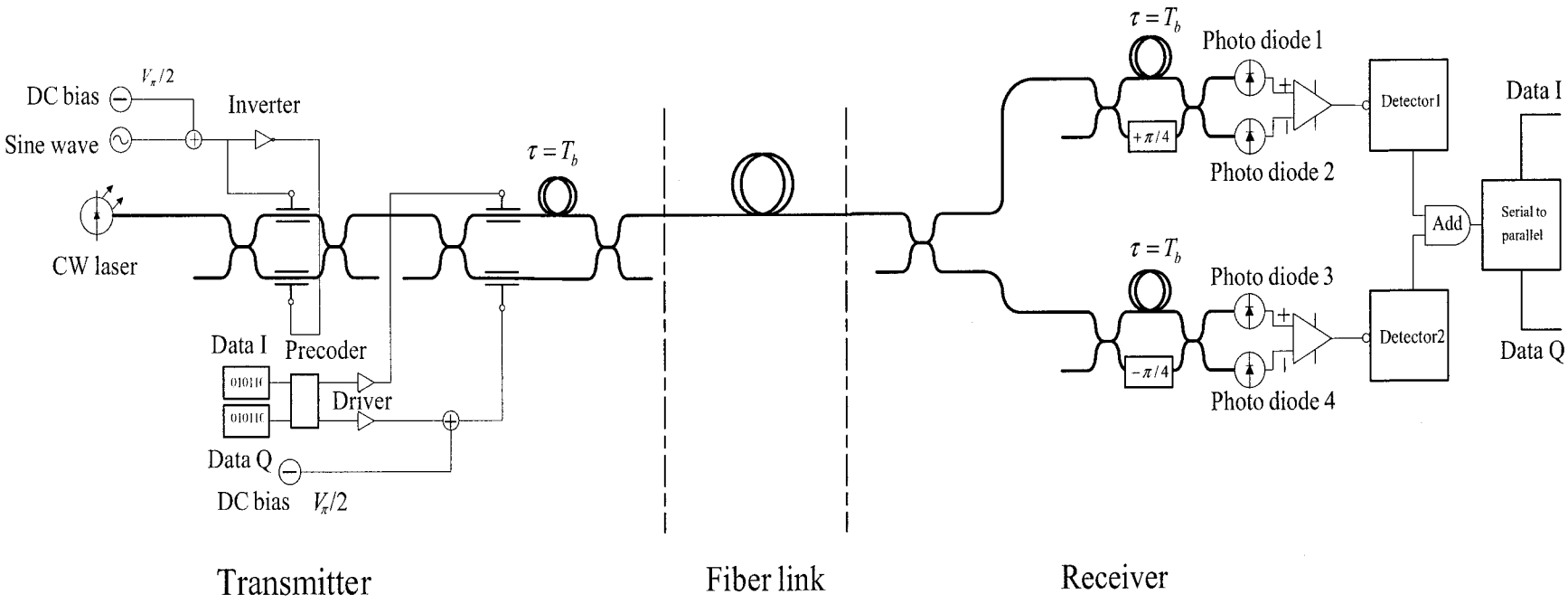

Figure 35: Schematic for Offset-DQPSK system model.

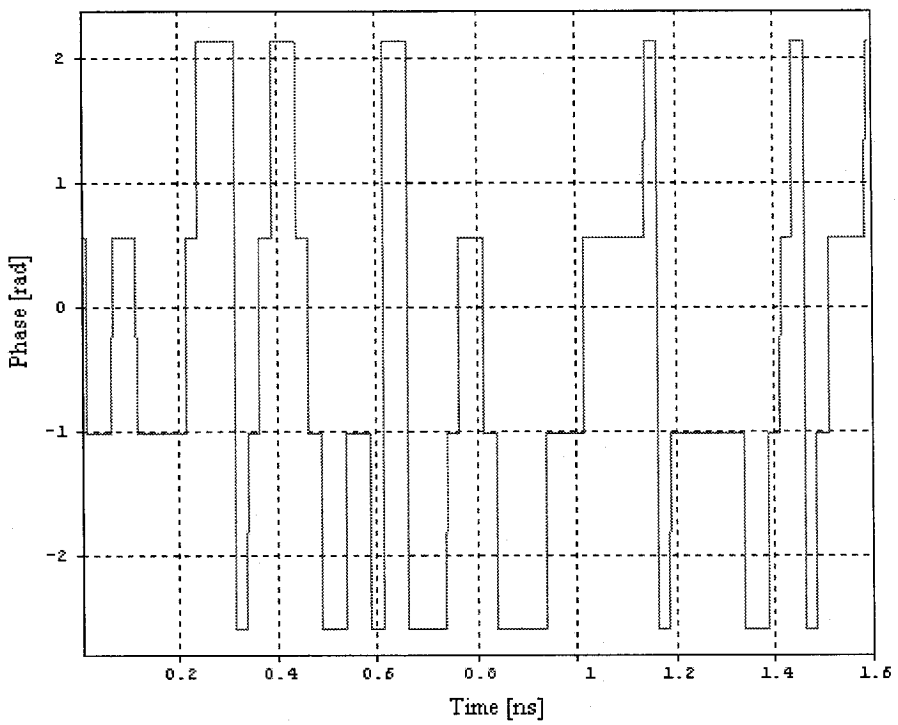

Figure 36: Line code of Offset-DQPSK with $\Delta\phi \in \{-\pi/2, 0, \pi/2\}$.

An orthogonal realization of Offset-DQPSK waveform is achieved by amplitude modulating the in-phase and quadrature data streams onto two carriers which have $\pi/2$ phase difference and 1 bit delay. Figure 37 depicts the structure of two optical Offset-DQPSK modulators. Figure 37 (a) uses a roll of fiber to implement one bit delay, and Figure 37 (b) uses a logic circuit to implement one bit delay. Both methods give same optical performance. Note that the bit rates of data I and data Q are half of the bit rates of the whole transmission system.

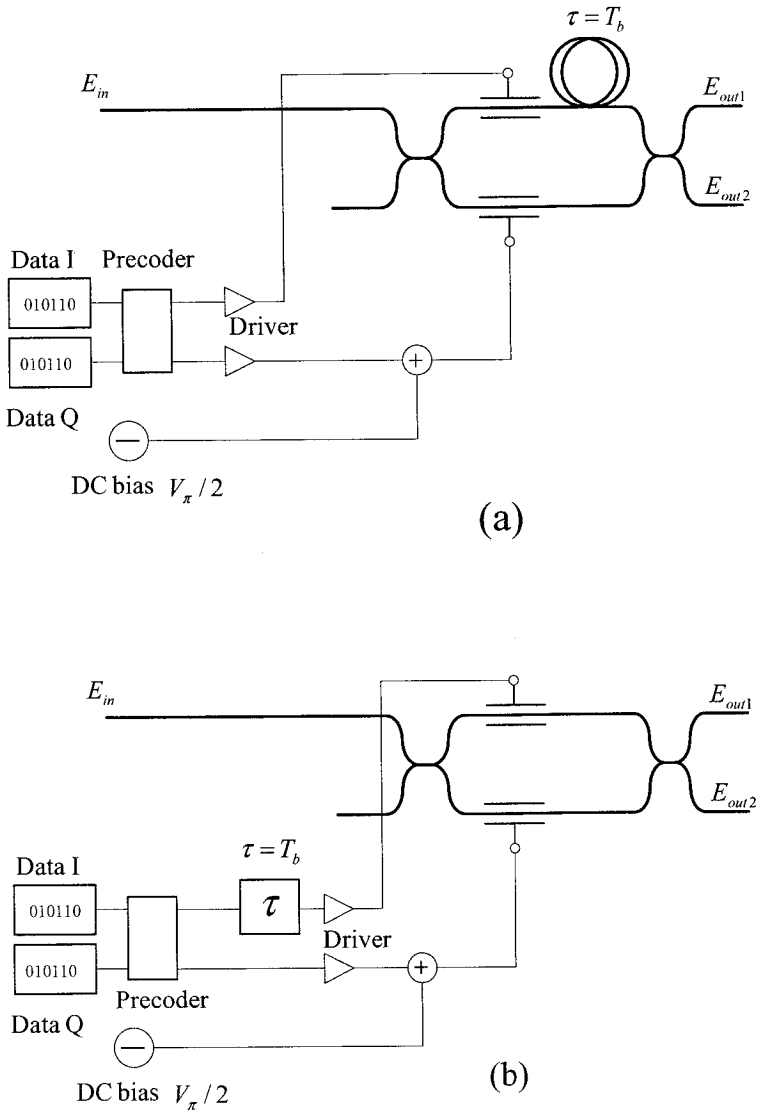

Figure 37: Schematic of Offset-DQPSK modulator by using (a) optical delay line, (b) logical delay circuit.

In Figure 37 (a), a MZM modulator is driven by two branches of data of information. One arm of the modulator biased by $V_\pi / 2$ voltage, gives a $\pi / 2$ phase shift, and the other arm of modulator has a 1 bit delay line. In Figure 37 (b), a MZM modulator is driven by two branches of data of information. One arm of the modulator biased by $V_\pi / 2$ voltage, gives a $\pi / 2$ phase shift. An one bit delay logic in one data branch is

used just after the precoder. In these two conditions, Equation (2.6) can be written

$$E_{out} = E_{in} \sin\left(\frac{\theta_1 - \theta_2}{2} - \frac{\pi}{4}\right) \exp\left(j\frac{\theta_1 + \theta_2}{2} + \frac{\pi}{4}\right) \tag{3.9}$$

Where E_{in} is electric field of laser carrier, θ_1 and θ_2 are two phase shifts corresponding to inphase and quadrature data, and both θ_1 and θ_2 belong to the set of $(0,\pi)$. Here we only account one output arm for simplicity. We can see the exact phase change of E_{out} depends on not only the exponential term but also the sine term of Equation (3.9). Figure 38 shows the phase constellation of Offset-DQPSK signal. We note that two half periods of phase shifts can not change simultaneously, and (π,π) situation is diminished.

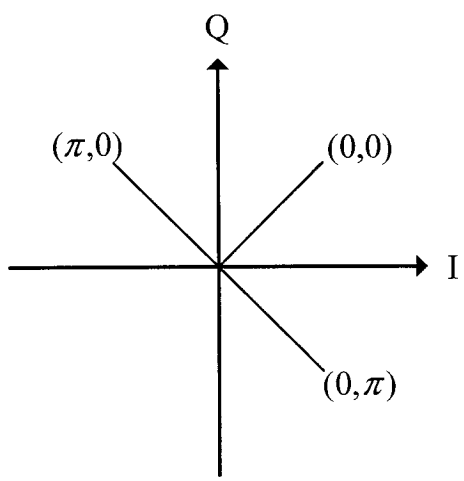

$$\sin\left(\frac{\theta_1 - \theta_2}{2} - \frac{\pi}{4}\right) \exp\left(j\frac{\theta_1 + \theta_2}{2} + \frac{\pi}{4}\right)$$

Figure 38: Phase constellation of ODQPSK.

Figure 39 shows the receiver of Offset-DQPSK. Two methods are given here, Figure 39 (a) use one MZI and Figure 39 (b) use two MZI. Two methods have slightly different optical performance. They have the same transmission logic; therefore we

can use the same precoder in the transmitter.

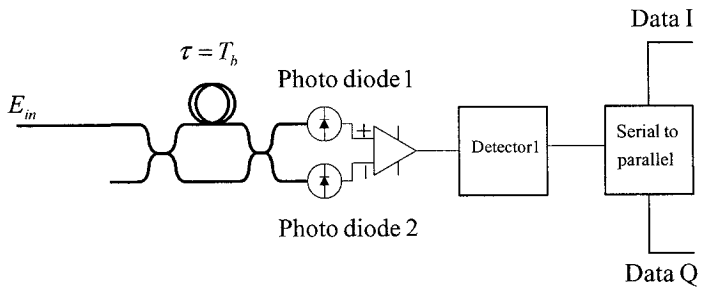

(a)

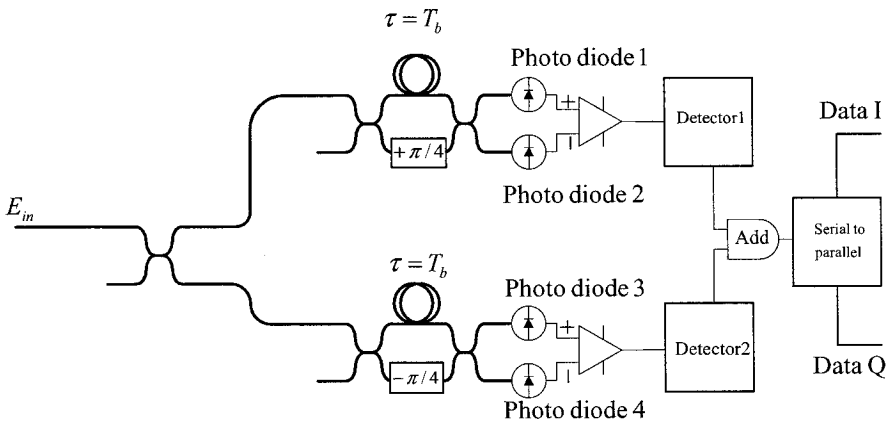

(b)

Figure 39: Schematic of Offset-DQPSK receiver with (a) one-branch demodulator, and (b) two-branch demodulator.

In Figure 39 (a), the demodulator is quit similar with the π-DPSK demodulator, and Equation (3.2) still works in this condition. In Figure 39 (b) the demodulator is quite similar with the DQPSK demodulator, and Equation (3.7) still works in this condition. A logical serial-to-parallel converter is required corresponding to two branch input data of information.

We compare the Q value performance of these two Offset-DQPSK demodulators by simulation. The simulation result shows that two-branch demodulator has approximately 2 dB better than one-branch demodulator in Q factor. Roughly speaking, the reason is that one- branch demodulator has $\pi/2$ symbol distance, while two-branch demodulator has $3\pi/4$ symbol distance.

3.42 Electronic precoder for Offset-DQPSK

In Offset-DQPSK system, the inphase and quadrature phase shift do not take place at the same time. We can simply consider that inphase and quadrature data do not interfere each other. Based on this fact, we give electronic precoder for Offset-DQPSK shown in Figure 40. Each branch works like an independent π-DPSK transmission. This conclusion comes from [38].

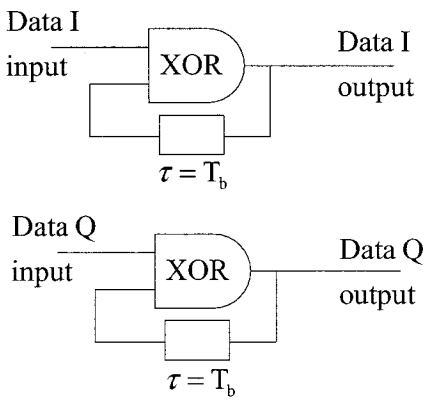

Figure 40: Schematic of electronic precoder for Offset-DQPSK.

Chapter 4

Comparison of system performances

The simulation was carried out to compare variant of performances of π-DPSK, $\pi/2$-DPSK, DQPSK and Offset-DQPSK. These performances include power spectrum, tolerance to fiber nonlinear effect, tolerance to fiber chromatic dispersion, tolerance to narrowband optical filtering. Following parameters are used except stated otherwise.

Reference bit rates of data: 40 Gb/s

Laser frequency/wavelength: 194 THz/1545.32 nm

FWHM of laser line width: 10 MHz

Simulation bandwidth frequency/wavelength: 0.8 THz/6.37 nm

Simulation samples per bit: 25

Total simulated time span: 16 ns

Total simulated bits: 640

Optical representation: single polarization

4.1 Comparison of power spectrum

Optical signal power spectrum gives the most important information of the lightwave system. It estimates bandwidth occupancy, and side band suppression ratio (SBSR), which are valuable parameters in system design tradeoffs. Figure 41 to 44 give the simulation result of π-DPSK, $\pi/2$-DPSK, DQPSK and Offset-DQPSK.

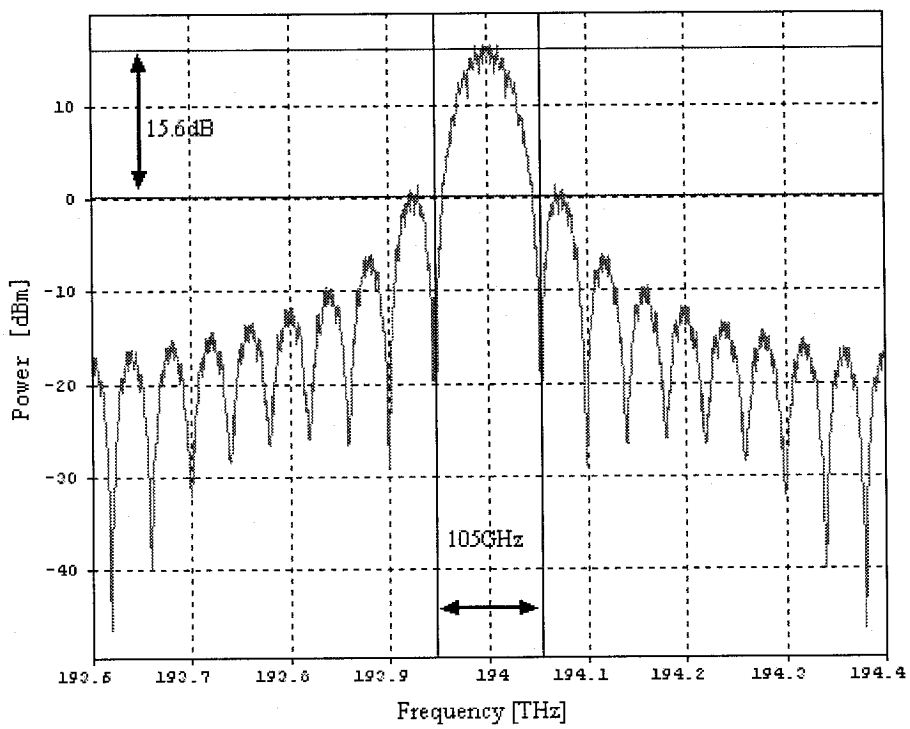

Figure 41: Optical power spectrum of π-DPSK.

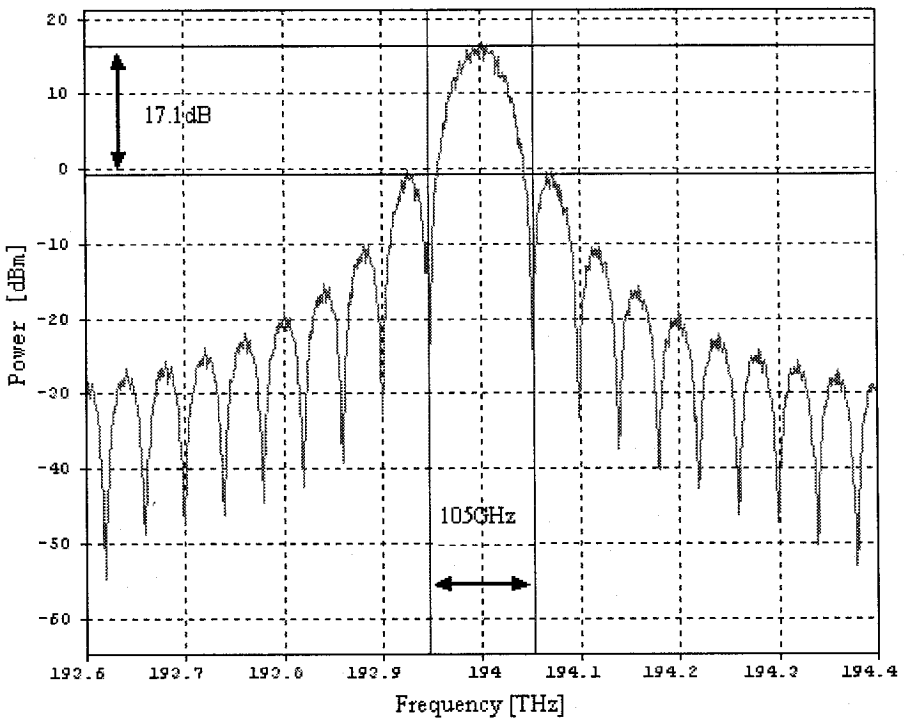

Figure 42: Optical power spectrum of $\pi/2$-DPSK.

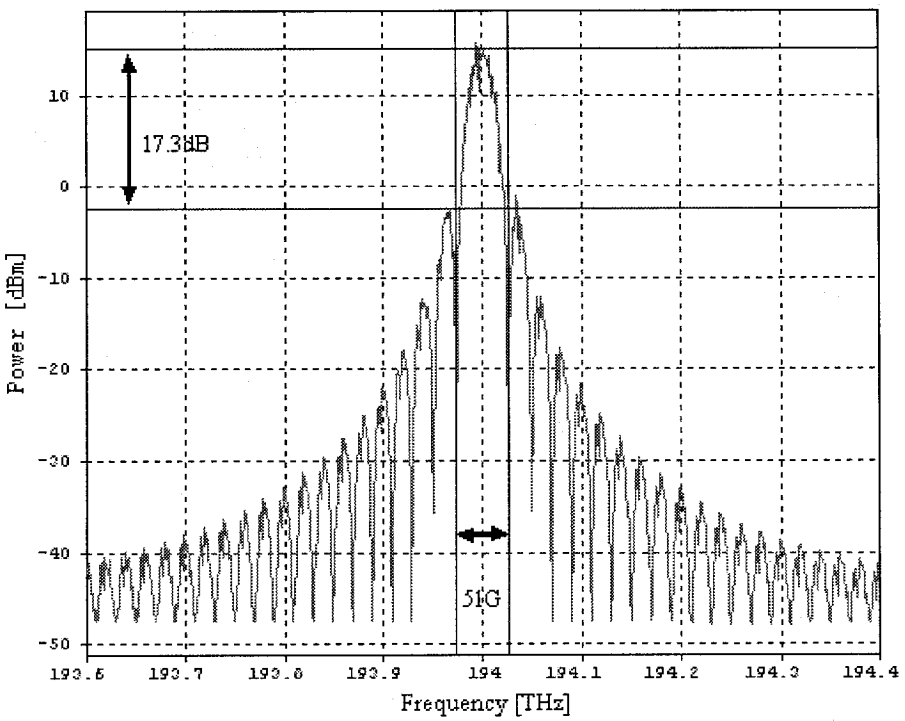

Figure 43: Optical power spectrum of DQPSK.

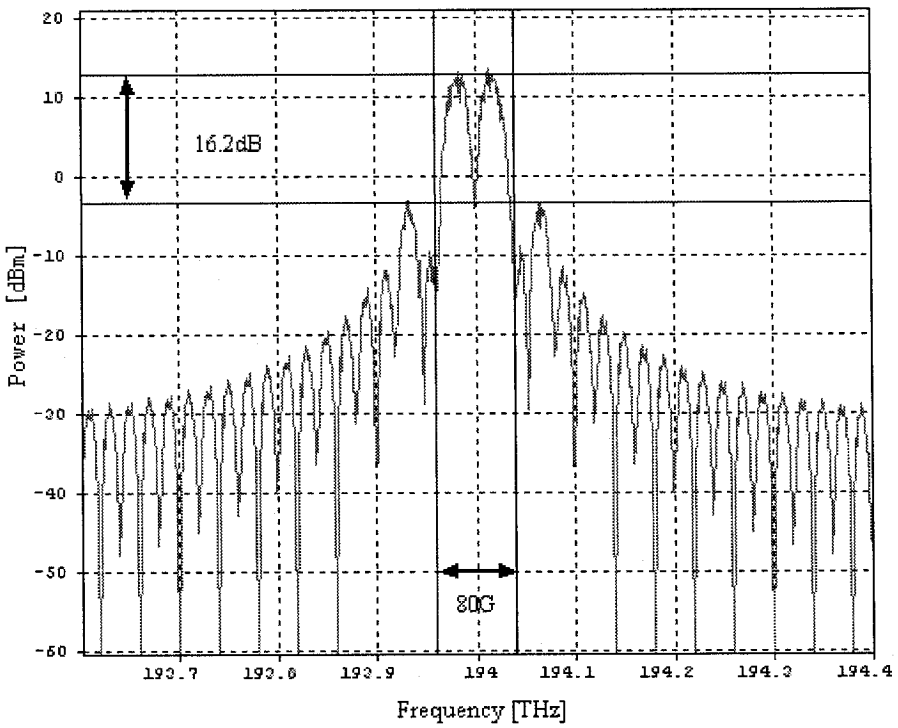

Figure 44: Optical power spectrum of Offset-DQPSK.

Table 4 Comparison of power spectrum

	π-DPSK	$\pi/2$-DPSK	DQPSK	O-DQPSK
Null to null bandwidth	105 GHz	105 GHz	51 GHz	80 GHz
SBSR	15.6	17.1	17.3	16.2

Table 4 lists the null to null bandwidth and side band suppression ratio (SBSR) measured in Figures 41 to 44. We can see that π-DPSK, $\pi/2$-DPSK have the same null to null bandwidth, while $\pi/2$-DPSK has higher side band suppression ratio than π-DPSK. DQPSK has the narrowest bandwidth among four phase modulation schemes. CSRZ Offset-DQPSK has two main lobes.

4.2 Comparison of optimum launched power under fiber nonlinear effect.

The intensity dependence of the refractive index in nonlinear optical media occurs through self-phase modulation, a phenomenon that leads to spectral broadening of optical pulses. Therefore inter symbol interference was induced as a factor of system performance degradation. Nonlinear effect also introduces strong phase noise by beating with ASE, but here we only discuss ISI effect.

Figure 45 shows the link configuration, which consists of a variable optical attenuation, 100km single mode fiber (SMF), 20km dispersion compensation fiber (DCF), a lumped optical amplifier, and an optical filter.

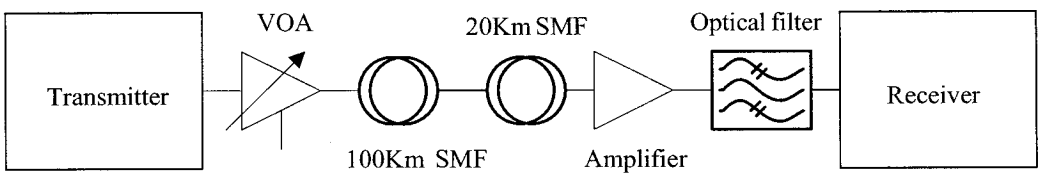

Figure 45: Schematic of transmission line for performance simulation.

Following parameters are used except stated other wise:

Lunched power: sweeping from -10 dBm to 20 dBm

Length of SMF: 100 km

Loss of SMF: 0.2 dB/km

Reference frequency for dispersion for SMF: 194 THz/1545.32 nm

Dispersion at the reference frequency for SMF: 16 ps/nm/km

Length of DCF: 20 km

Loss of DCF: 0.2 dB/km

Reference frequency for dispersion for DCF: 194 THz/1545.32 nm

Dispersion at the reference frequency for DCF:-80 ps/nm/km

Flat gain of lumped amplifier: 24 dB

Number of poles of Bessel optical filter: 2

Center frequency of Bessel optical filter: 194 THz/1545.32 nm

-3dB Bandwidth of Bessel optical filter: 60 GHz

Figures 46 to 49 show the simulation result of π-DPSK, $\pi/2$-DPSK, DQPSK and Offset-DQPSK.

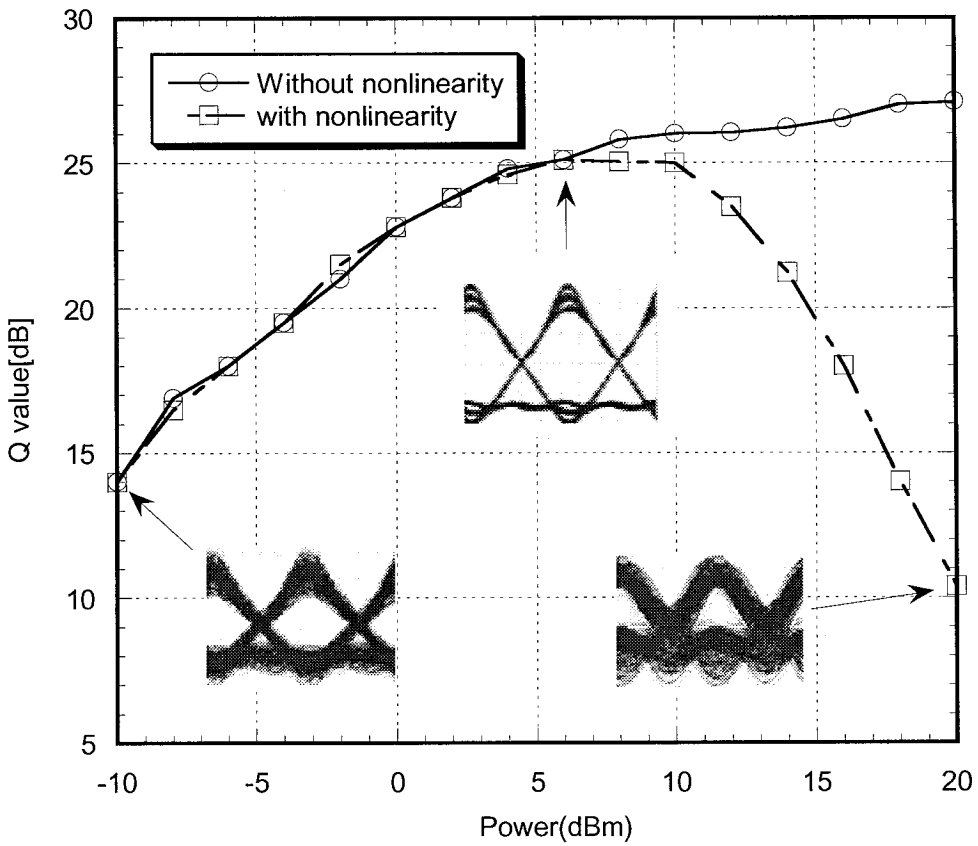

Figure 46: Q value vs. launched power for π-DPSK.

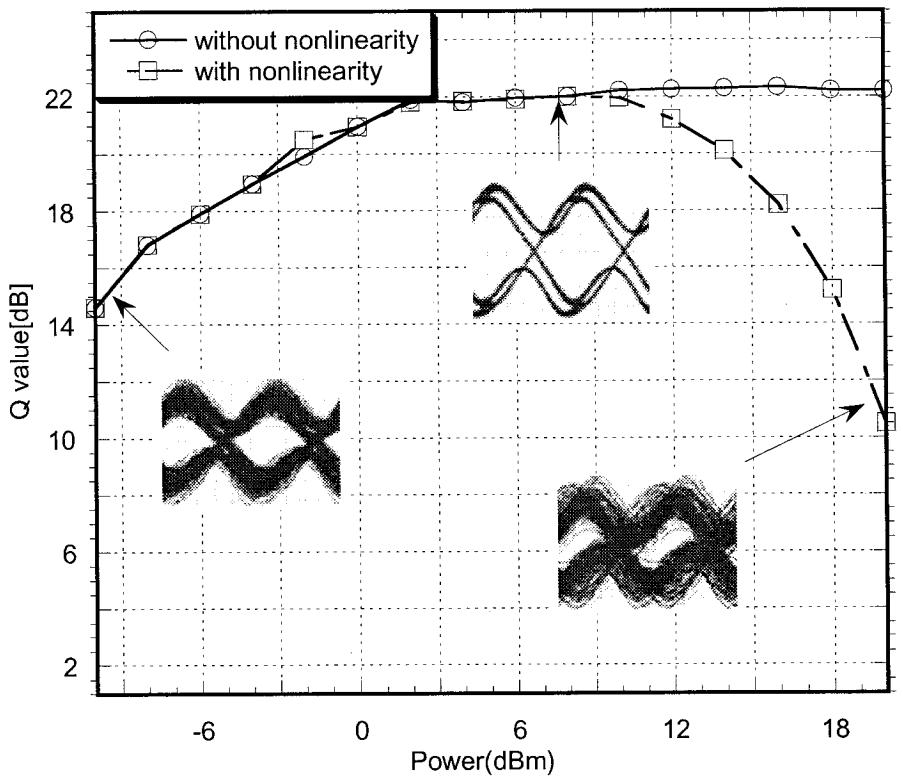

Figure 47: Q value vs. launched power for $\pi/2$-DPSK.

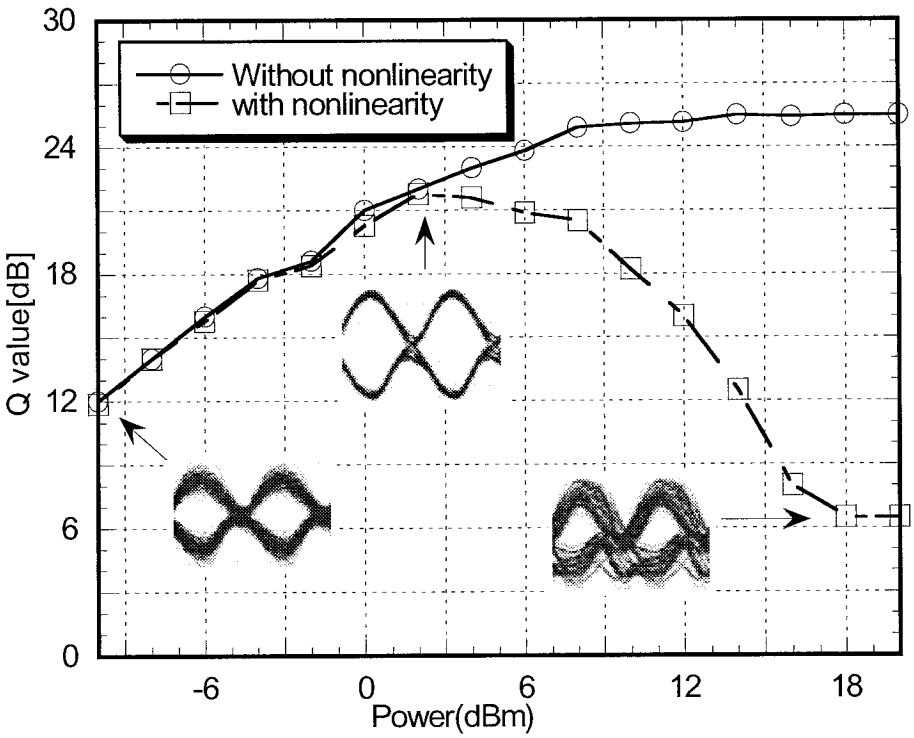

Figure 48: Q value vs. launched power for DQPSK.

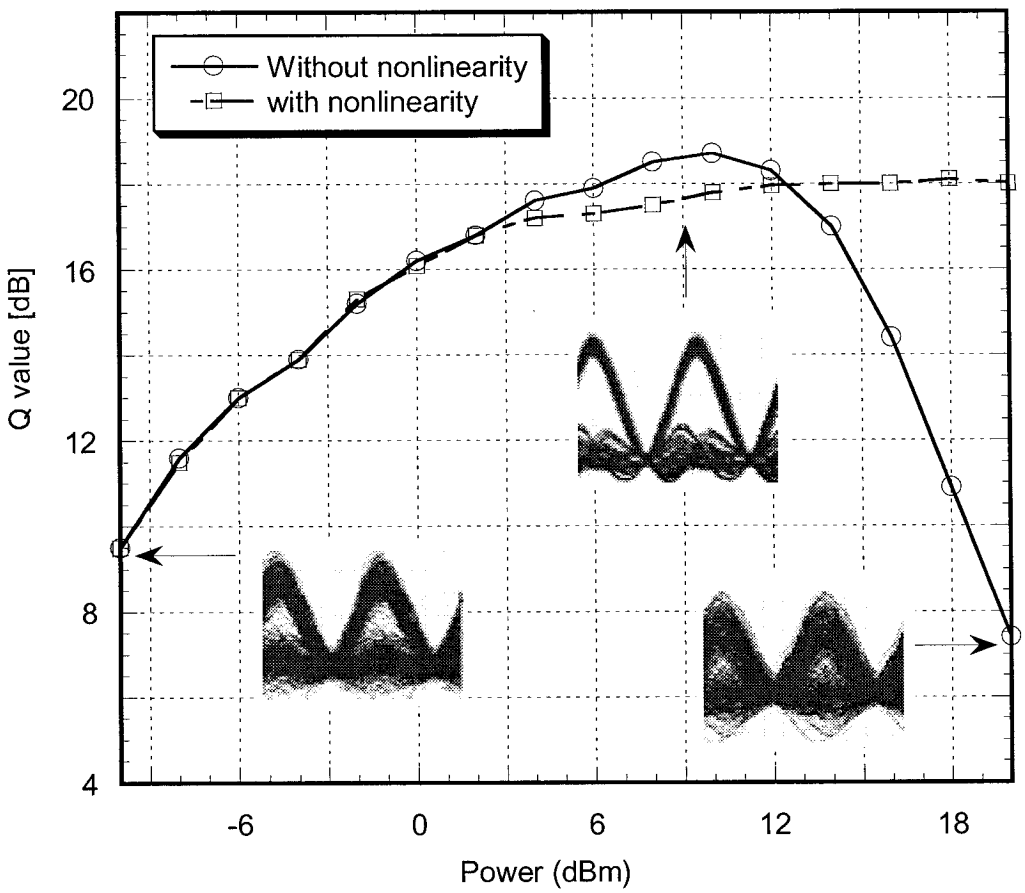

Figure 49: Q value vs. launched power for Offset-DQPSK.

Table 5 Comparison of optimum launched power under fiber nonlinear effect.

	π -DPSK	$\pi/2$ -DPSK	DQPSK	O-DQPSK
Optimum launched power	6 dBm	8 dBm	4 dBm	10 dBm
Q	25.2 dB	22.1 dB	22 dB	18.5 dB

Table 5 lists the optimum launched power and corresponding Q value measured in

Figures 46 to 49.

We can see that Offset-DQPSK has the best potential of tolerance to ISI induced by fiber nonlinear effect.

4.3 Comparison of tolerance to optical filtering

DWDM long haul transmission link at high speed usually suffers from severe narrow band optical channel composed of a series of optical add-drop multiplexers. And optical filters used in the optical fiber link serve two purposes, one is to reduce the amplifier noise, and the other is to suppress the side band spectra of light wave. So the optical channel will introduce strong ISI. Trade off is necessary to balance these effects.

Figure 45 shows the link configuration, which consists of a variable optical attenuation, 100 km single mode fiber, 20km dispersion compensation fiber, a lumped optical amplifier, a variable-bandwidth optical filter.

Following parameters are used:

Lunched power: Optimum power in Table 4.5

Length of SMF: 100 km

Loss of SMF: 0.2 dB/km

Reference frequency for dispersion for SMF: 194 THz/1545.32 nm

Dispersion at the reference frequency for SMF: 16 ps/nm/km

Length of DCF: 20 km

Loss of DCF: 0.2 dB/km

Reference frequency for dispersion for DCF: 194 THz/1545.32nm

Dispersion at the reference frequency for DCF:-80 ps/nm/km

Flat gain of lumped amplifier: 24 dB

Number of poles of Bessel optical filter: 2

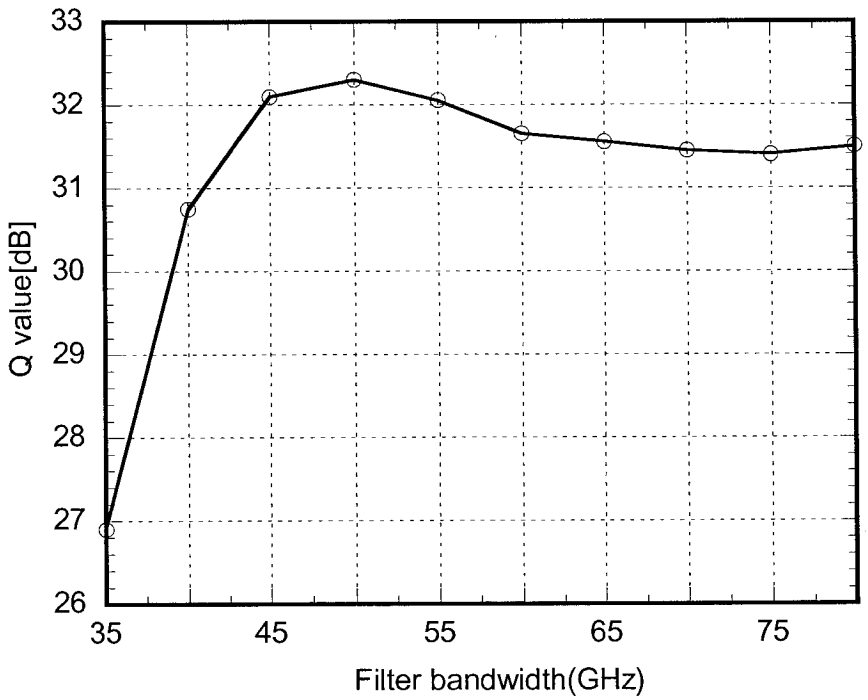

Figure 50: Q value vs. optical filter bandwidth for π-DPSK.

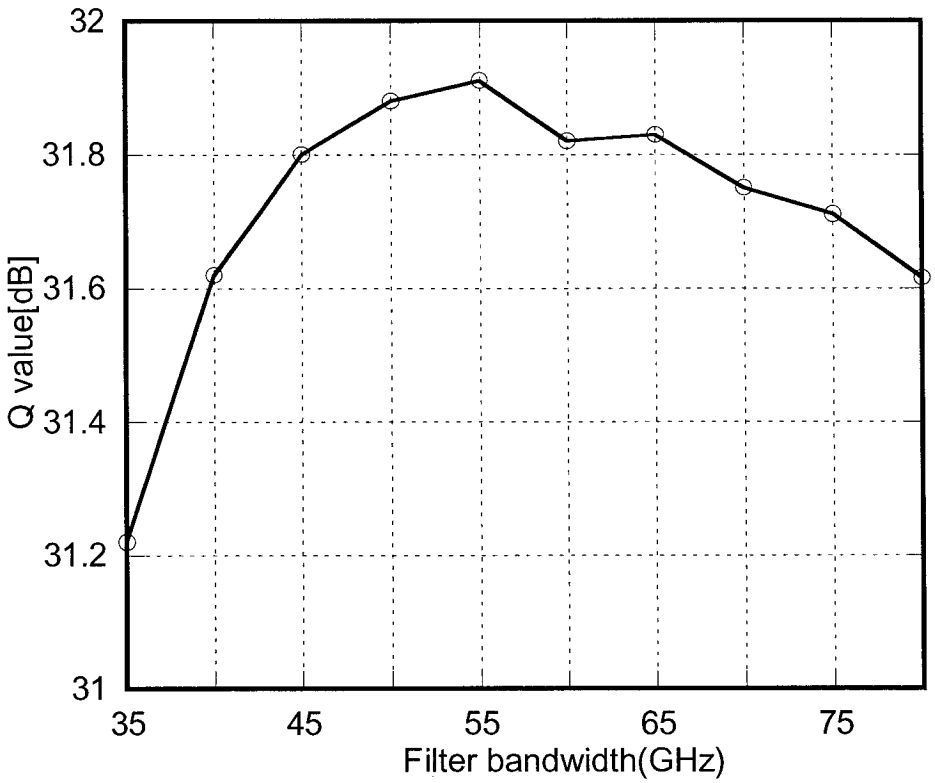

Figure 51: Q value vs. optical filter bandwidth for $\pi/2$-DPSK.

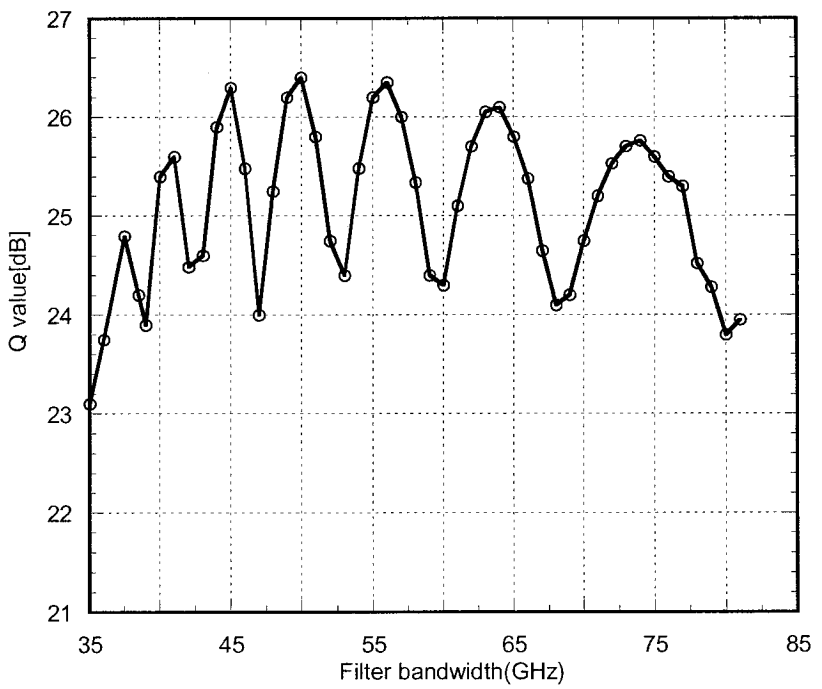

Figure 52: Q value vs. optical filter bandwidth for DQPSK.

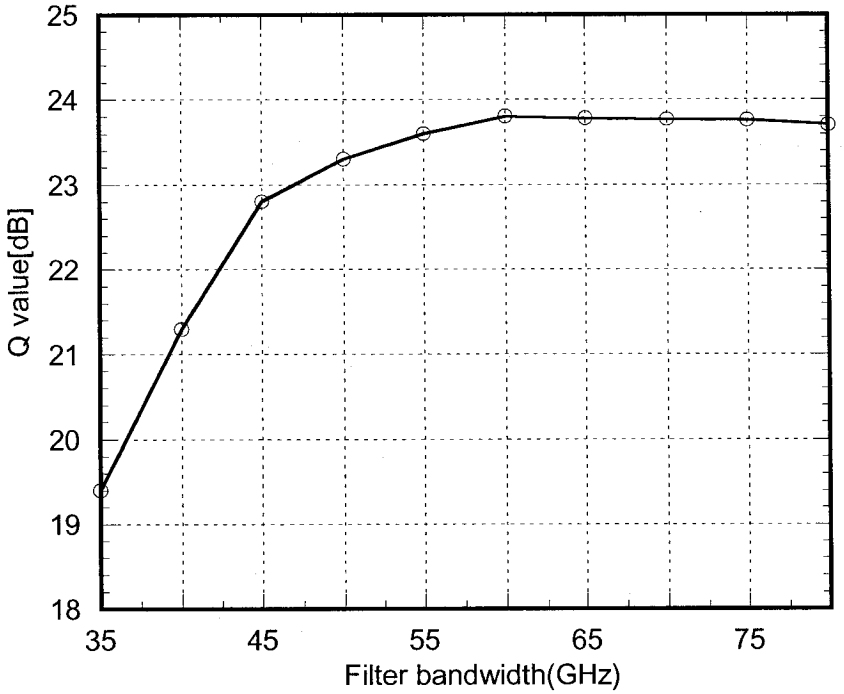

Figure 53: Q value vs. optical filter bandwidth for Offset-DQPSK，.

Center frequency of Bessel optical filter: 194 THz/1545.32 nm

-3dB Bandwidth of Bessel optical filter: sweeping from 35 GHz to 80 GHz

Figures 50 to 53 show the simulation result of π-DPSK, $\pi/2$-DPSK, DQPSK and Offset-DQPSK.

Table 6 Comparison of tolerance to optical filtering

	π-DPSK	$\pi/2$-DPSK	DQPSK	Offset-DQPSK
Optimum 3dB Bandwidth	50GHz	55GHz	NA	60

Table 6 lists the optimum 3-dB bandwidth measured in Figures 49 to 52. We can see

π-DPSK has the best tolerance to optical filtering. DQPSK has an oscillated curve along the optical filter bandwidth.

4.4 Comparison of tolerance to residual chromatic dispersion (CD)

Chromatic dispersion is one of the major limiting factors of modern optical communication system. Figure 45 shows the link configuration, which consists of a variable optical attenuation, 100km single mode fiber, 20km dispersion compensation fiber, a lumped optical amplifier, and an optical filter.

Following parameters are used:

Lunched power: 0 dBm

Length of SMF: 100 km

Loss of SMF: 0.2 dB/km

Reference frequency for dispersion for SMF: 194 THz/1545.32 nm

Dispersion at the reference frequency for SMF: 16 ps/nm/km

Length of DCF: 20 km

Loss of DCF: 0.2 dB/km

Reference frequency for dispersion for DCF: 194 THz/1545.32 nm

Dispersion at the reference frequency for DCF: sweeping from -80 to 73 (ps/nm/km)

Flat gain of lumped amplifier: 24 dB

Number of poles of Bessel optical filter: 2

Center frequency of Bessel optical filter: 194 THz/1545.32 nm

-3dB Bandwidth of Bessel optical filter: 60 GHz

Figure 54 shows the simulation result of π-DPSK, $\pi/2$-DPSK, DQPSK and

Offset-DQPSK.

We can see from Figure 54 that DQPSK has the best tolerance to residual chromatic dispersion simply because it has the narrowest null to null band width. π-DPSK has better tolerance to residual chromatic dispersion than $\pi/2$-DPSK.

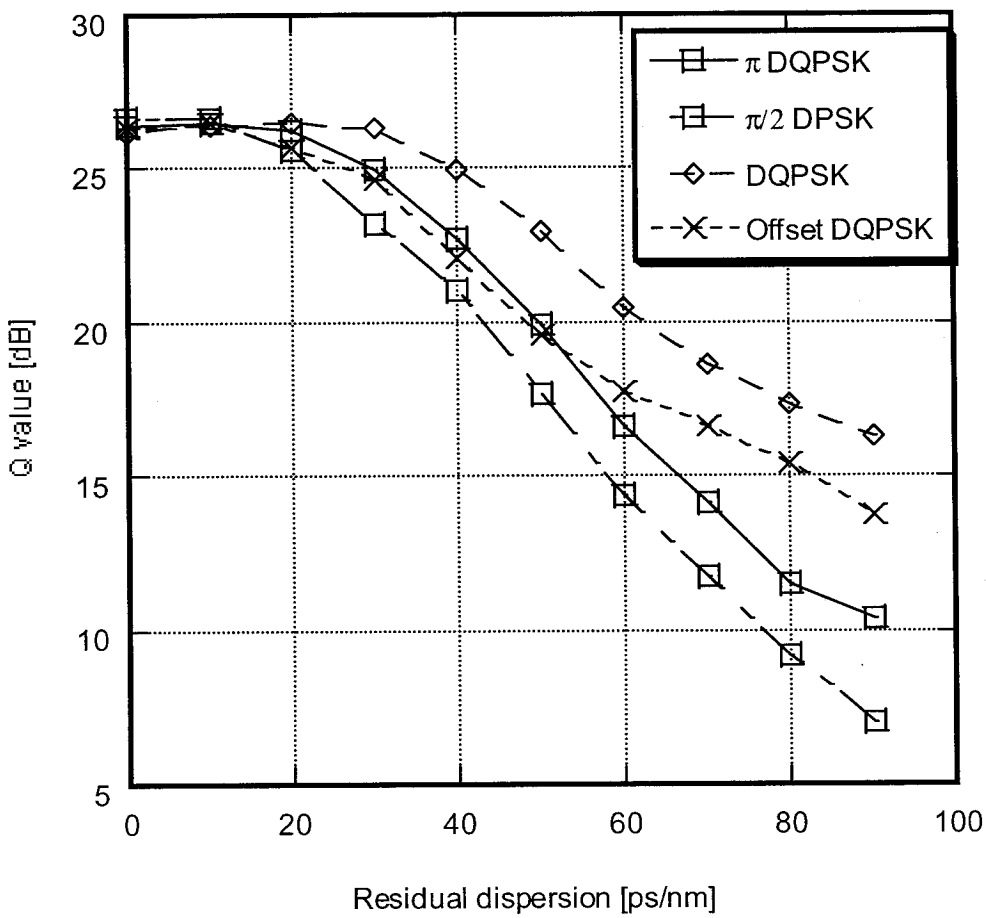

Figure 54: Comparison of tolerance to residual chromatic dispersion

Chapter5

Conclusion

High speed optical π-DPSK, $\pi/2$-DPSK, DQPSK and Offset-DQPSK were investigated thoroughly. The logic and basic circuit of electronic precoder of optical $\pi/2$-DPSK were presented in this thesis. We found that π-DPSK, $\pi/2$-DPSK have the same null to null bandwidth; $\pi/2$-DPSK has higher side band suppression ratio than π-DPSK; DQPSK has the narrowest bandwidth among four phase modulation schemes; Offset-DQPSK has two main lobes; and Offset-DQPSK has the best potential of tolerance to ISI induced by fiber nonlinear effect. π-DPSK has the best tolerance to optical filtering. DQPSK performance is oscillated with the optical filter bandwidth. DQPSK has the best tolerance to residual chromatic dispersion.

Some theoretical analyses are not given in this thesis, and we leave them open for our future work.

Appendix A

Simulation platform: Optism

OptSim is an optical communication system simulation package designed for engineering and research of WDM, DWDM, TDM, CATV, optical LAN, parallel optical bus, and other emerging optical systems in telecom, datacom, and other applications. It can be used to design optical communication systems and simulate them to determine their performance given various component parameters. OptSim is designed to combined the accuracy and modeling. It includes the most component models and simulation algorithms.

OptSim represents an optical communication system as an interconnected set of blocks, with each block representing a component or subsystem in the communication system. As physical signals are passed between components in a real world communication system, "signal" data is passed between component models in the OptSim simulation. Each block is simulated independently using the parameters specified by the user for that block and the signal information passed into it from other blocks. This is known as a block-oriented simulation methodology. These blocks are graphically represented as icons in OptSim. Internally, they are represented as data structures and sophisticated numerical algorithms. OptSim fiber simulation is

based on the Time Domain Split-Step (TDSS) method. It is the new technology for optical system simulation and its advantages over Frequency-Domain Split-Step FDSS. This method takes into account all linear and non-linear effects, and is one of the most accurate methods available in the field of optical fiber propagation simulation.

OptSim includes an extensive component model library of the most commonly used components for the engineering of electro-optical systems. OptSim includes a new sophisticated yet easy-to-use graphical user interface (GUI), plus twin simulation engines, and powerful simulation result analysis and post-processing tools. The user interface provides a hierarchical object-oriented CAD environment for schematic development and system design.

Optism users may further augment the component library with your own custom components through our Custom Component as Executable (CCE) facility. You can generate an external executable, using any program language like C, C++, Fortran, Pascal, etc. that models your own component. During simulation OptSim and your CCE will exchange signals using the documented OptSim signal format.

Appendix B

Simulation setup in Optsim

Figure B.1 is simulation setup for π-DPSK transmission system. Figure B.2 is simulation setup for $\pi/2$-DPSK transmission system. Figure B.3 is simulation setup for DQPSK transmission system. Figure B.4 is simulation setup for Offset-DQPSK transmission system. These setups were verified in Optsim 4.0. Some components were co simulated with Mathlab 7.0.

All the simulation results in this thesis were carried out using these setups.

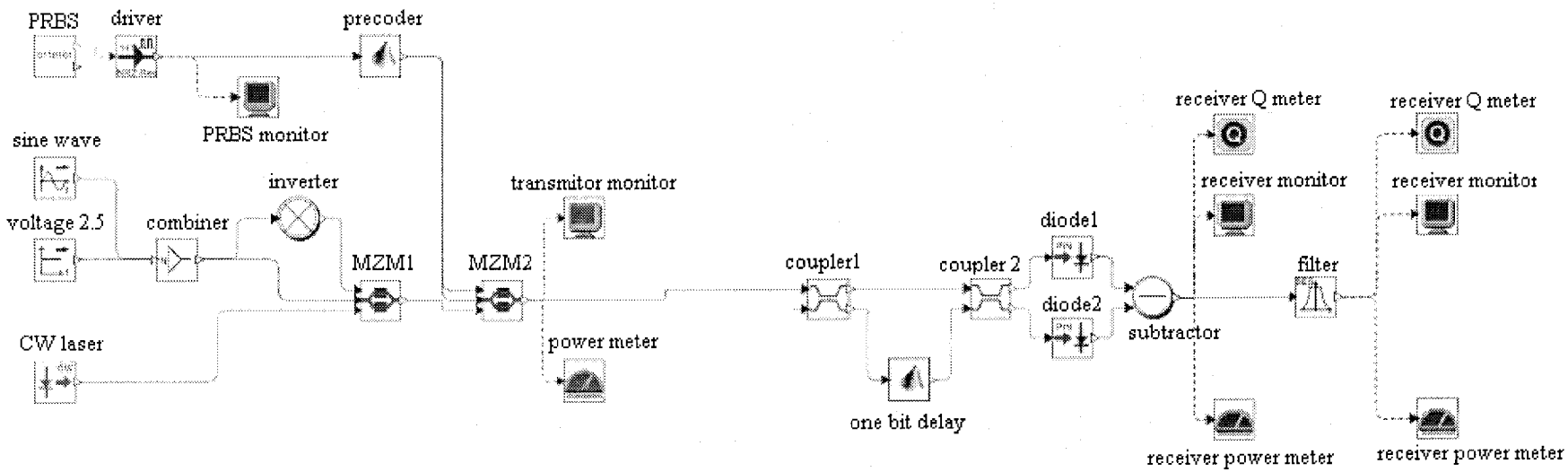

Figure B.1: Simulation setup for π DPSK.

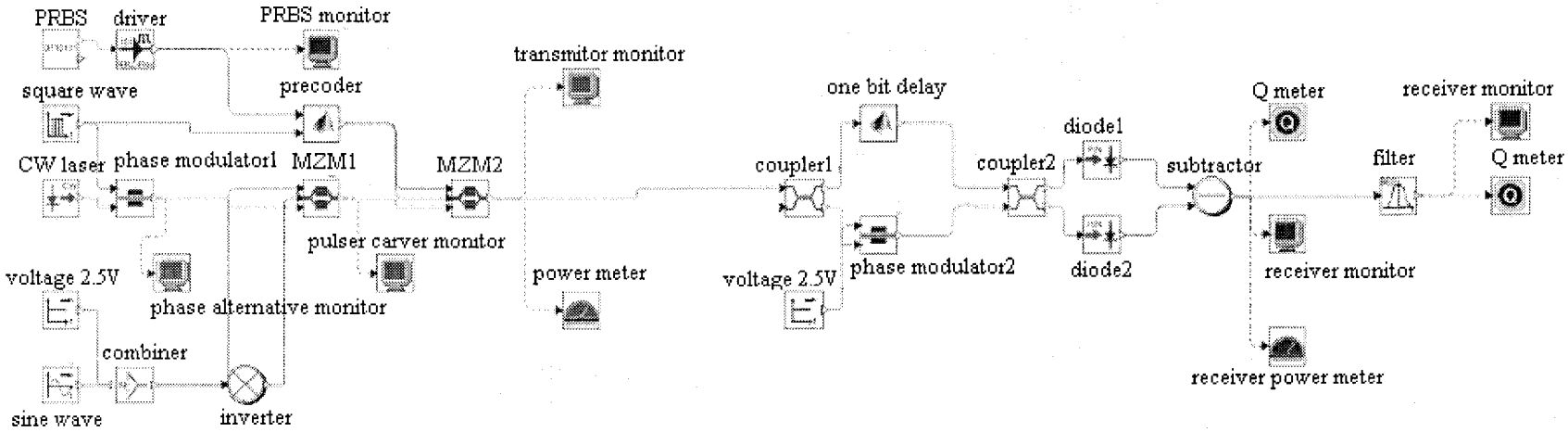

Figure B.2: Simulation setup for $\pi/2$ DPSK.

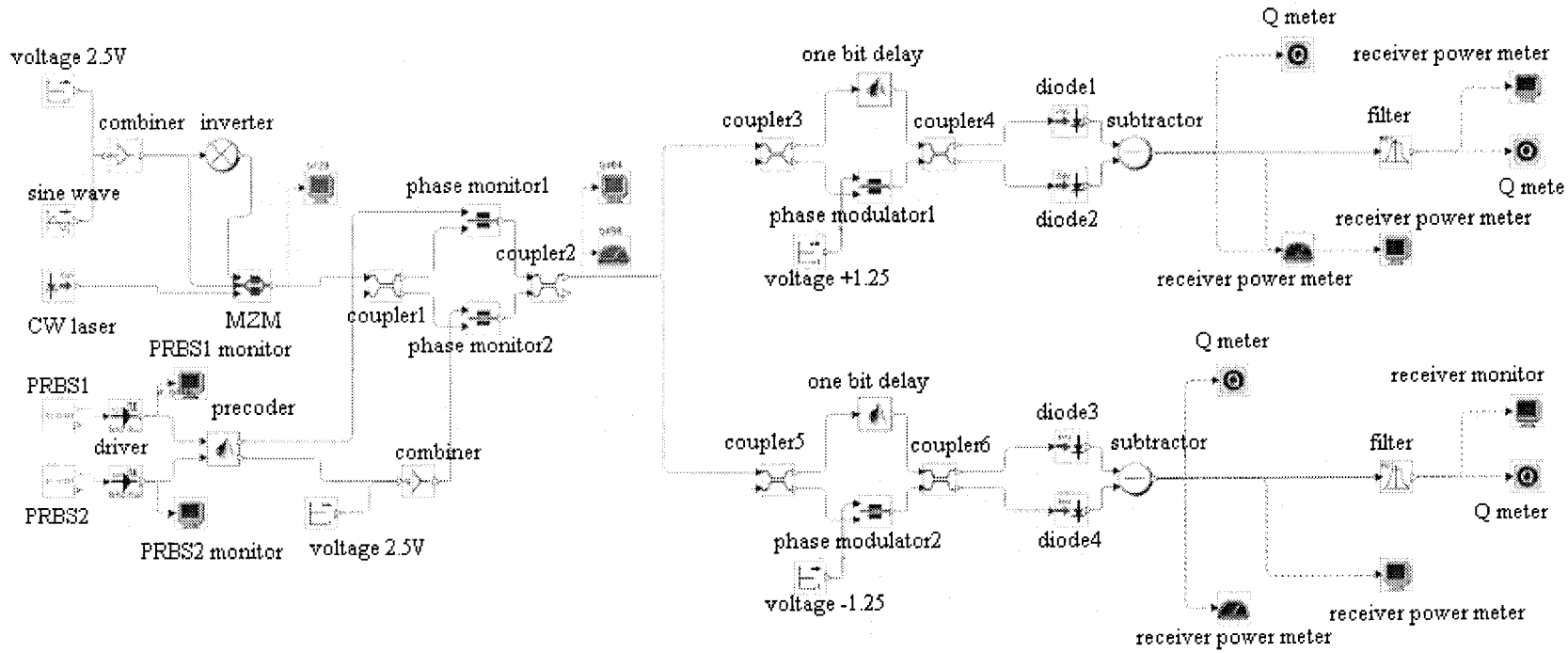

Figure B.3: Simulation setup for DQPSK

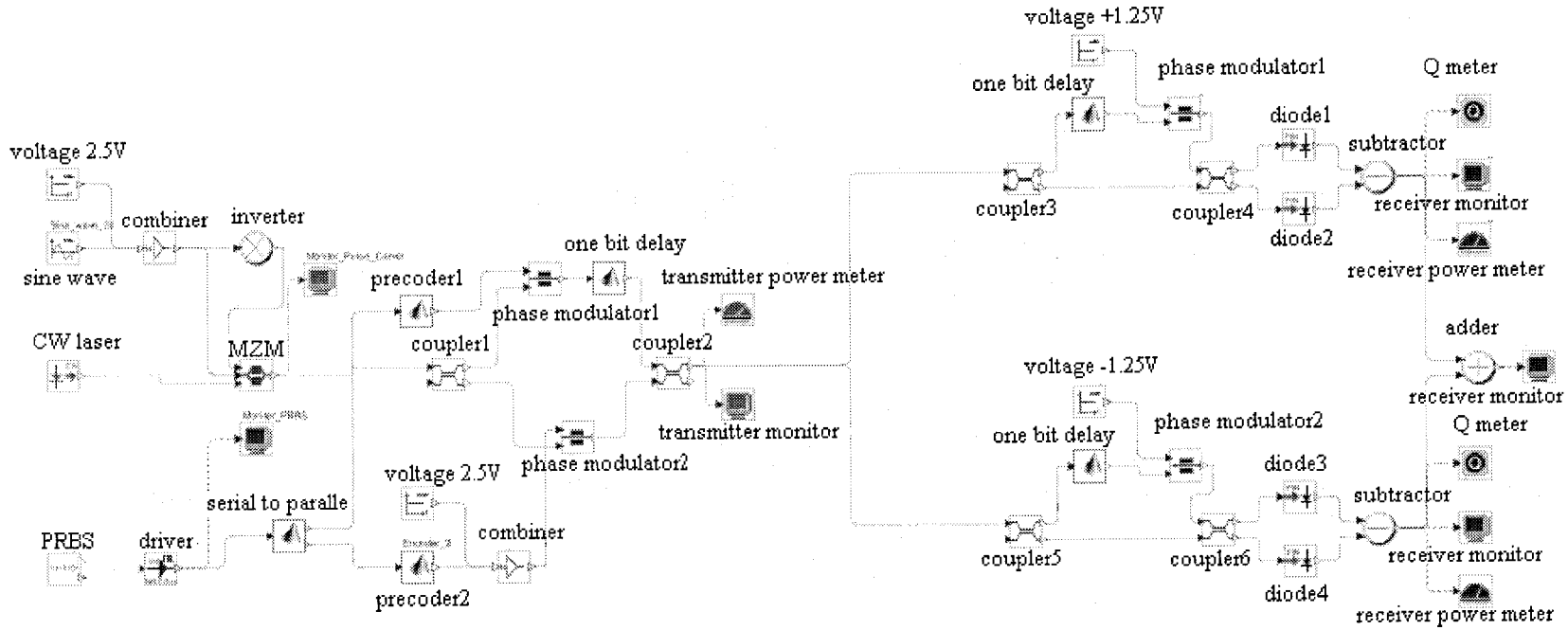

Figure B.4: Simulation setup for offset DQPSK.

Reference

[1] Yonenaga K. and Kuwano S., "Dispersion-tolerant optical transmission system using duobinary transmitter and binary receiver," *J. Lightwave Tech., Vol. 15, pp.1530 -1537, 1997.*

[2] Yonenaga, K., Yoneyama, M., Miyamoto, Y., Hagimoto, K. Noguchi, "160-Gbit/s WDM transmission experiment using four 40-Gbit/s optical duobinary channels," *OFC 1998, Technical Digest, pp. 49 -51.*

[3] Gu, X., Dodds, S.J., Blank, L.C., Spirit, D.M. Pycock, S.J.; Ellis, A.D., "Duobinary technique for dispersion reduction in high capacity optical systems-modeling, experiment and field trial," *IEEE Proceedings-Optoelectronics Vol. 143, pp. 228 -236, 1996.*

[4] Djupsjobacka, A., "Prechirped duobinary modulation," *IEEE Photonics Tech. Lett., Vol . 10, pp. 1159 -1161, 1998.*

[5] Ono, T., Yano, Y., Fukuchi, K., Ito, T., Yamazaki, H., Yamaguchi, M., Emura, K.,

"Characteristics of optical duobinary signals in terabit/s capacity, high-spectral efficiency WDM systems," *J. Lightwave Tech., Vol. 16, pp. 788 -797, 1998.*

[6] Penninckx D., Chbat M., Pierre L., Thiery J.-P., "The phase-shaped binary transmission (PSBT): a new technique to transmit far beyond the chromatic dispersion limit," *IEEE Photon. Tech. Lett., Vol. 9, pp. 259 -261, 1997.*

[7] Charlet G., Lanne S., Pierre L., Simonneau, C., Tran P. Mardoyan H., Brindel P., Antona J., Molina M., Godin J., Bigo S., "Cost-optimized 6.3 Tb/s capacity terrestrial link over 17x100km using phase shaped binary transmission in a conventional all-EDFA SMF-based system," *OFC 2003, PD25.*

[8] Bosco, G., Carena, A., Curri, V., Gaudino, R., Poggiolini, P., "On the use of NRZ, RZ, and CSRZ modulation at 40 Gb/s with narrow DWDM channel spacing," *J. Lightwave Tech., Vol. 20, pp. 1694 –1704, 2002.*

[9] Lee J., Kim S., Kim Y., Oh Y., Hwang S., Jeong J., "Optically preamplified receiver performance due to VSB filtering for 40-Gb/s optical signals modulated with various formats," *J. Lightwave Tech., Vol. 21, pp. 521 -527, 2003.*

[10] Zhu Y., Lee, Scahill C., Watley D., Fludger C., Bontemps P., Jones M., Pettitt G., Shaw B., Hadjifotiou A., "16-channel 40 Gb/s carrier-suppressed RZ ETDM/DWDM transmission over 720 km NDSF without polarization channel interleaving," *OFC 2001, Vol. 4, ThF4.*

[11] Miyamoto Y., Yonenaga K., Kuwahara S., Tomizawa M., Hirano A., Toba H., Murata K., Tada Y., Umeda Y., Miyazawa H., "1.2 Tbit/s (30×42.7 Gbit/s ETDM optical channel) WDM transmission over 376 km with 125 km spacing using forward error correction and carrier-suppressed RZ format," *OFC 2000 , Vol.4 , pp.245 -247.*

[12] Miyamoto Y., Kuwahara S., Hirano A., Tada Y., Yamane Y., Miyazawa H., "Reduction of nonlinear crosstalk by carrier-suppressed RZ format for 100 GHz-spaced Nx43-Gbit/s WDM in non-zero dispersion shifted band," *ECOC 2001. Vol. 4, pp. 528 -529.*

[13] Leibrich J., Wree C., Rosenkranz W., "CF-RZ-DPSK for suppression of XPM on dispersion-managed long-haul optical WDM transmission on standard single-mode fiber," *IEEE Photon. Tech. Lett., Vol. 14, pp. 155 -157, 2002.*

[14] Winzer P., Chandrasekhar S., Kim H., "Impact of filtering on RZ-DPSK reception," *IEEE Photon. Tech. Lett., Vol. 15, pp. 840 -842, 2003.*

[15] Gnauck A., Raybon G, Chandrasekhar S., Leuthold J., Doerr C., Stulz L., Agarwal A., Banerjee S., Grosz D., Hunsche S., Kung A., Marhelyuk A., Maywar D., Movassaghi M., Liu X., Xu C., Wei X., Gill D., "2.5 Tb/s (64/spl times/42.7 Gb/s) transmission over 40/spl times/100 km NZDSF using RZ-DPSK format and all-Raman-amplified spans," *OFC 2002, FC2.*

[16] Hoshida T., Vassilieva O., Yamada K., Choudhary S., Pecqueur R., Kuwahara H.,

"Optimal 40 Gb/s modulation formats for spectrally efficient long-haul DWDM systems," *J. Lightwave Tech., Vol. 20, pp. 1989 -1996, 2002.*

[17] Xu C., Liu X., Mollenauer L., Wei X., "Comparison of return-to-zero differential phase-shift keying and ON-OFF keying in long-haul dispersion managed transmission," *IEEE Photon. Tech. Lett., Vol. 15, pp. 617 -619, 2003.*

[18] Gnauck A., Raybon G., Chandrasekhar S., Leuthold J., Doerr C., Stulz L., Burrows E., "25x40-Gb/s copolarized DPSK transmission over 12x100-km NZDF with 50-GHz channel spacing," *IEEE Photon. Tech. Lett., Vol. 15, pp. 467 -469, 2003.*

[19] Rasmussen C., Fjelde T., Bennike J., Liu F., Dey S., Mikkelson B., Mamyshev P., "DWDM 40G transmission over trans-pacific distance (10,000km) using CSRZ-DPSK, enhanced FEC and all-Raman amplified 100 km Ultra Wave fiber spans," *OFC 2003, PD18.*

[20] Zhu B., Nelson L., Stulz S., Gnauck A., Doerr C., Leuthold J., Gruner-Nielsen L, Pedersen M., Kim J., Lingle R., Emori Y., Ohki Y., Tsukiji N., Oguri A., Namiki S., "6.4 Tb/s (160x42.7Gb/s) transmission with 0.8 bit/s/Hz spectral efficiency over 32x100 km of fiber using CSRZ-DPSK format," *OFC 2003, PD19.*

[21] Marcerou J., Vareille G., Becouarn L., Pecci P., Tran P., "8370 km with 22dB spans ULH transmission of 185x10.709Gb/s RZ-DPSK channels," *OFC 2003, PD20.*

[22] Cai J., Foursa D., Davidson C., Cai Y., Domagala G., Li H., Liu L., Patterson W., Pilipetskii A., Nissov M., Bergano N., "A DWDM demonstration of 3.73 Tb/s over 11,000 km using 373 RZ-DPSK channels at 10 Gb/s," *OFC2003, PD22.*

[23] Tsuritani T., Agata A., Morita I., Edagawa N., Ishida K., Shimomura K., Tokura T., Mizuochi T., Taga H., "70 GHz-spaced 40x42.7 Gb/s transmission over 8700 km using CSRZ-DPSK signal, all Raman repeaters and symmetrically dispersion-managed fiber span," *OFC 2003, PD23.*

[24] Ishida K., Kobayashi T., Abe J., Kinjo K., Kuroda S., Mizuochi T., "A comparative study of 10 Gb/s RZ-DPSK and RZ-ASK WDM transmission over transoceanic distance," *OFC 2003, ThE2.*

[25] Hirano A., Miyamoto Y., Kuwahara S., "Performance of CSRZ-DPSK and RZ-DPSK in 43-Gb/s/ch DWDM G.652 single-mode fiber transmission," *OFC 2003, ThE4.*

[26] Jin Wang, Joseph M. Kahn, "Conventional DPSK versus symmetrical DPSK: comparison of dispersion tolerances," *IEEE Photon. Tech. Lett., Vol.16, No.6, Jun. 2004.*

[27] Douglas M.Gill, Xiang Liu, Xing Wei, Sonali Banerjee, "$\pi/2$ Alternate-Phase ON-OFF keyed 40-Gb/s transmission on standard Single-Mode fiber," *IEEE Photon. Tech. Lett., Vol.15, No.12, Dec 2003.*

[28] X..Wei, A.H.Gnauck, "Optical $\pi/2$-DPSK and its tolerance to filtering and polarization-mode dispersion," *IEEE Photon. Tech. Lett., Vol.15, No.11, Nov. 2003.*

[29] Ut-Va Koc, Xing Wei, "Combined effect of polarization-Mode dispersion and chromatic dispersion on strongly filtered $\pi/2$-DPSK and conventional DPSK," *IEEE Photon. Tech. Lett., Vol. 16, Jun. 2004.*

[30] Hoon Kim, Rene-Jean Essiambre, "Transmission of 8x20 Gb/s DQPSK signals over 310 km SMF with 0.8-b/s/Hz spectral efficiency," *IEEE Photon. Tech. Lett., Vol.15 No.5, May. 2003*

[31] R.A.Griffin, A.C. Carter, "Optical differential quadrature phase-shift key for high capacity optical transmission," *OFC 2002, WX6.*

[32] R.Griffin, R. Johnstone,R. Walker, S. Wadsworth, A. Carter, " Integrated DQPSK transmitter for dispersion-tolerant and dispersion-managed DWDM transmission," *OFC 2003, FP6.*

[33] O.Vassilieva, T.Hoshida, S.Choudhary, H.Kuwahara, "Non-linear tolerant and spectrally efficient 86 Git/s RZ-DQPSK format for a system upgrade," *OFC 2003, ThE7.*

[34] Pak S. Cho, Vladimir S. Grigoryan, "Transmission of 25 Gb/s RZ-DQPSK

signals with 25 GHz channel spacing over 1000 km of SMF-28 fiber," *IEEE Photon. Tech. Lett., Vol. 15, No.3. Mar. 2003.*

[35] R.A. Griffin, R.I. Johnstorn, R.G. Walker,J. Hall, S.D. Wadsworth, K.Berry, A.C. Carter,M.J. Wale, "10 Gb/s optical differential quadrature phase shift key transmission using GaAs/AlGaAs integration," *OFC 2002, FD6-1, Post deadline Papers.*

[36] C.Wree, J. Leibrich, J. Eick, W. Rosenkranz, "Experimental investigation of receiver sensitivity of RZ-DQPSK modulation format using balanced detection," *OFC 2003, ThE5.*

[37] Christoph Wree, Murat Serbay, Jochen Leibrich, Werner Rosenkranz, "Offset-DQPSK modulation format for 40Gb/s and comparison to RZ-DQPSK in WDM environment," *OFC 2003, MF62.*

[38] Koffi Defly, Michel Lecours, "Differential detection of the OQPSK signal: coding ad decoding".

[39] Marvin K. Simon, Charles c. Wang, "Differential detection of Gaussian MSK in a mobile radio environment," *IEEE Trans. VEH. Technol., Vol. VT-33 No.4, Nov. 1984.*

[40] Joan M.Gene, Marcal Soler, Robert I. Killey, and Josep Prat, "Investigation of 10-Gb/s optical DQPSK systems in presence of chromatic dispersion, fiber

nonlinearities, and phase noise," *IEEE. Photon. Tech. Lett., Vol. 16, No.3, Mar. 2004.*

[41] I. Korn, "Offset DPSK with differential phase detector in satellite mobile channel with narrow-band receiver filter," *IEEE. Trans. Veh. Technol., Vol. 38, pp. 193–203, Nov. 1989.*

[42] J. H. Winters, "Differential detection with intersymbol interference and frequency uncertainty," *IEEE Trans. Commun., Vol. COM-32, pp. 25–33, Jan. 1984.*

[43] Kathsushi Iwashita, Takao Matsumoto, "Modulation and detection characteristics of optical continuous phase FSK transmission system," *J. Lightwave Tech., Vol. T-5, No.4 Apr. 1987.*

[44] A.Hirano, Y.Miyamoto, S.Kuwahara, "Performances of CSRZ-DPSK and RZ-DPSK in 43 Gb/s/ch DWDM G652 single-mode fiber Transmission," *OFC 2003 ThE4.*

[45] Govind P.Agrawal "Nonlinear fiber optics," *Academic Press 3rd Edition.*